A NEW APPLICATION OF THE CHANNEL PACKET METHOD FOR LOW ENERGY 1-D ELASTIC SCATTERING

THESIS

Clint M. Zeringue, Second Lieutenant, USAF

AFIT/GAP/ENP/06-22

**DEPARTMENT OF THE AIR FORCE
AIR UNIVERSITY**

AIR FORCE INSTITUTE OF TECHNOLOGY

Wright-Patterson Air Force Base, Ohio

AFIT/GAP/ENP/06-22

A NEW APPLICATION OF THE CHANNEL PACKET METHOD FOR LOW ENERGY 1-D ELASTIC SCATTERING

THESIS

Presented to the Faculty

Department of Engineering Physics

Graduate School of Engineering and Management

Air Force Institute of Technology

Air University

Air Education and Training Command

In Partial Fulfillment of the Requirements for the

Degree of Master of Science (Applied Physics)

Clint M. Zeringue, BS

Second Lieutenant, USAF

September 2006

AFIT/GAP/ENP/06-22

**A NEW APPLICATION OF THE CHANNEL PACKET METHOD FOR LOW
ENERGY 1-D ELASTIC SCATTERING**

Clint M. Zeringue, BS
Second Lieutenant, USAF

Approved:

_____   _____
David E. Weeks (Chairman)   date

_____   _____
Thomas A. Niday (Member)   date

_____   _____
William F. Bailey (Member)   date

Abstract

An algorithm is presented which uses the channel packet method (CPM) to compute S-matrix elements. The standard approach to solving for the S-matrix elements is to use states which contain only positive or negative momentum. In doing so however, the standard approach fails to produce accurate S-matrix elements at low energies since accurate results are only obtainable over the energy range defined by the states. Therefore, in order to obtain accurate results at low energy one must formulate states which contain both positive and negative momentum. In order to incorporate states which have positive and negative momentum a four-by-four matrix containing the momentum expansion coefficients of the states is introduced. The approach does not consider scattering from one side or the other, rather it considers both incoming and outgoing states from the left and right simultaneously. Therefore, during one simulation all four S-matrix elements, $S_{+k,-k}, S_{-k,+k}, S_{+k,+k}$ and $S_{-k,-k}$ are computed. Numerical simulations of the algorithm are carried out on a conventional desktop computer and compared to the analytic solution of the transmission and reflection functions for a square and trapezoidal well. The simulated results agree very well with the known solution up until very low energies, after which the results begin to oscillate about the theoretical values. The explanation of the oscillations is presented as well as two error analyses: the first showing that the oscillations approach zero as the reactant and product wave packets are propagated away from the interaction region, and the second showing convergence to the correct S-matrix elements for a trapezoidal well. The results indicate that if the exact

Møller states are used the algorithm will produce the correct S-matrix elements across the

entire energy range.

Acknowledgments

I would like to express a sincere gratitude to my faculty advisor, Dr. David Weeks,

for his guidance and expertise throughout the work of this thesis. His enthusiastic

demeanor during our technical discussions made learning about scattering theory a joyful

experience.

A special thank you goes to my girlfriend for her constant love, compassion, and patience

throughout this thesis. I would like to thank her for understanding that even during visits

it may have seemed as though we were still apart during the intense research phase. I

would also like to thank my parents for always believing in my dreams and their

continued support for the choices I make.

Clint M. Zeringue

Table of Contents

List of Figures

x

List of Tables

A NEW APPLICATION OF THE CHANNEL PACKET METHOD FOR LOW ENERGY 1-D ELASTIC SCATTERING

I Introduction

1.1 Overview

On the highway, we try to avoid colliding with other cars. On the pool table, we tailor collisions to suit our purposes. In particle accelerators, we interpret collisions to reveal the innermost structure of matter. On a cosmic scale, we wonder if a collision between an asteroid and Earth led to the extinction of the dinosaurs. Collisions are important features of our physical universe.

Jay M. Pasachoff, *Physics* (1999)

Classical mechanics describes the properties and effects of various collisions through the conservation laws of energy and momentum. In the microscopic world however, one must adopt the theory of quantum mechanics to characterize the interactions between particles. In classical mechanics one only needs to specify the velocities and masses of the interacting constituents to completely characterize a collision; the quantum collision picture or "scattering theory", is a much more subtle affair. In quantum mechanics velocity and position are viewed in terms of probabilities. The purpose of collision theory in the quantum mechanical regime is then to calculate the probability that, as the result of a collision, a particle will "scatter," or deviate from its initial path. Scattering theory was developed to describe the statistical nature of microscopic collisions.

The Strahlung matrix (S-matrix) is the core of scattering theory. The S-matrix is a unitary matrix that relates the final state in the infinite future (out-channel) and the initial state in the infinite past (in-channel). The individual elements in the S-matrix are known as scattering amplitudes; squaring the modulus of the S-matrix elements produces the transmission and reflection probability coefficients T and R for an arbitrary potential $V(x)$. The channel packet method (CPM) is a time dependent approach to scattering theory that produces the S-matrix elements numerically.

Dr. David E. Weeks and Dr. David J. Tannor developed the CPM in the early 1990's. Tannor and Weeks used Møller operators to propagate reactant and product wave packets into interaction regions of step-like potential barriers and wells as well as a collinear reaction of atomic hydrogen and dihydrogen. The S-matrix elements were calculated through a Fourier transform of a time-dependent correlation function between the Møller states. Using the S-matrix elements Weeks and Tannor were able to produce transmission and reflection curves that agreed well with the known solutions. However, at low energies the results of their calculations deviated significantly from the theoretical predictions. [1-3]

A more complete algorithm, capable of yielding good results along the entire energy spectrum, is needed. The goal of this project is to explore 1-D, elastic scattering and apply a new approach to the CPM in an attempt to correct the errors that occur at low energies. A new algorithm is developed to approach the problem from a different perspective. Previous algorithms described in [1-3] contain a specific requirement- the reactant and product wave functions are formulated such that they have either all positive

or negative momentum. Weeks and Tannor showed that accurate results were only attainable over the range of momentum for which the amplitude of the product and reactant wave packets is nonzero. Since previous methods confined the momentum amplitude of the wave packets to go to zero near low momentum (and hence low energy) information was lost and as a result, deviations from the analytic solutions were observed in the low energy portions of the transition curves.

The objective of this thesis is to develop a new algorithm capable of producing better results in the low-energy limit. To achieve this objective we employ several adaptations to previous applications of the CPM. First, the product and reactant wave packets are constructed to contain both positive and negative momentum. As an effect of the previous requirement, scattering from the left and right is considered simultaneously, and the entire S-matrix is produced during a single propagation. Lastly, a significant increase in simulation time as well as grid size is required to propagate the product and reactant wave packets into the asymptotic channels. The last requirement stems from the first in that with both positive and negative momentum propagation out of the interaction region becomes more time consuming do to spreading of the wave functions in both directions. The nature of the approach taken in this thesis requires that the wave packets contain both positive and negative momentum. To truly propagate the wave packets completely out of the interaction region requires an infinite grid. Since this requirement cannot be met one must accept this limitation and attempt to propagate far enough so that the amplitude remaining inside the interaction region is negligible.

There are two main contributions presented in this thesis: an algorithm that produces a significant improvement in the reflection and transmission curves at low energies, and a program developed to analytically solve for the transmission and reflection coefficients for a trapezoidal well. In addition, the explanations of problematic results at low energies are characterized.

1.2 **Organization**

This thesis begins with a description of the scattering matrix and a summary of the CPM in Section 2. This section is designed for those who have studied basic quantum mechanics but have had no exposure to the CPM. It discusses a derivation of the scattering matrix, the Møller operators, the split-operator, how to formulate the reactant and product wave packets, and the approach to calculate the S-matrix from the correlation functions. I attempt to make the discussion clearer by explaining how these topics are applied to a square well scattering problem. In section 3, the requirements of the previous algorithm developed in [1-3] are discussed as well as explanations of why the algorithm fails at low energy.

The new algorithm developed in this thesis is then presented with a focus on discussing how it will result in significant improvements in the low energy regime. Section 4 then describes the parameters of a typical CPM simulation as well as the implications of changing them. In section 5 the results of low energy scattering are presented for a square well. Some of the difficulties encountered are discussed as well as the convergence rate of the error associated with a discrete square well based on the coordinate grid spacing. Section 6 discusses the first of two error analyses; the

methodology behind the error analysis is presented along with the results. Sections 7 and

8 discuss the trapezoidal well as well as the second error analysis showing that the S-

matrix elements produced by the new algorithm converge to the correct solution in the

low energy regime. Finally, a summary of the thesis is presented as well as

recommendations for future research.

II   Time Dependent Scattering Theory

2.1   The S-Matrix

As noted earlier the scattering matrix is related to the transmission and reflection coefficients introduced in a basic quantum mechanics course. To demonstrate the relationship I will adopt a problem from *An Introduction to Quantum Mechanics* by David J. Griffiths [4]. Consider an arbitrary, localized potential

$$V(x) = \begin{cases} 0 & x < -a \\ V(x) & -a \le x \le a, \\ 0 & x > a \end{cases} \tag{1}$$

shown in Figure 1. In region I $V(x) = 0$, so

$$\psi(x) = Ae^{ikx} + Be^{-ikx}, \quad where \quad k = \frac{\sqrt{2mE}}{\hbar} \tag{2}$$

and in region III $V(x)$ again is zero, so

$$\psi(x) = Fe^{ikx} + Ge^{-ikx}. \tag{3}$$
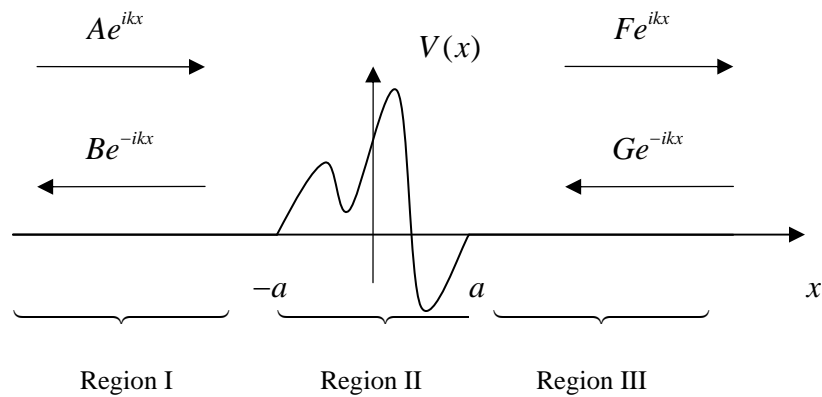
Figure 1. Scattering from an arbitrary localized potential ($V(x) = 0$ except in Region II)

In Region II, ψ cannot be determined until the potential is specified, but because the Schrödinger equation is a linear, second-order differential equation, the general solution has to be of the form

$$\psi(x) = Cf(x) + Dg(x),\tag{4}$$

where $f(x)$ and $g(x)$ are two linearly independent particular solutions [5]. There will be four boundary conditions:

$$\begin{aligned}
\psi_1(-a) &= \psi_2(-a)\\
\psi'_1(-a) &= \psi'_2(-a)\\
\psi_2(a) &= \psi_3(a)\\
\psi'_2(a) &= \psi'_3(a)
\end{aligned}\tag{5}$$

where the subscript indices 1, 2, and 3 stand for the three regions. Two of these boundary conditions can be used to eliminate C and D, and the other two can be "solved" for B and F in terms of A and G:

$$B = S_{+k,-k}A + S_{-k,-k}G,\tag{6}$$

and

$$F = S_{+k,+k}A + S_{-k,+k}G.\tag{7}$$

The four coefficients $S_{\pm k,\pm k}$ depend on k (and hence E) and constitute the 2×2 S-matrix. The S-matrix tells you the outgoing amplitudes (B and F) in terms of the incoming amplitudes (A and G):

$$\begin{pmatrix} B \\ F \end{pmatrix} = \begin{pmatrix} S_{+k,-k} & S_{-k,-k} \\ S_{+k,+k} & S_{-k,+k} \end{pmatrix}\begin{pmatrix} A \\ G \end{pmatrix}\tag{8}$$

Considering only scattering from the left ($G = 0$);

7

$$R_l = \frac{|B|^2}{|A|^2}\bigg|_{G=0} = \left|S_{+k,-k}\right|^2, \quad T_l = \frac{|F|^2}{|A|^2}\bigg|_{G=0} = \left|S_{+k,+k}\right|^2, \qquad (9)$$

or from the right ($A = 0$),

$$R_r = \frac{|F|^2}{|G|^2}\bigg|_{A=0} = \left|S_{-k,+k}\right|^2, \quad T_r = \frac{|B|^2}{|G|^2}\bigg|_{A=0} = \left|S_{-k,-k}\right|^2 \qquad (10)$$

where the subscripts l and r denote scattering from left and right respectively. Any

realistic scattering experiment will consist of sending a beam of particles into the

interaction region. The beam will have some spread in energy (hence momentum) and

thus cannot be represented as a plane wave. To handle the spread, Gaussian wave

packets are used to represent the (inbound) and (outbound) states. In the more realistic

picture, equation (8) will take on a more complicated form consisting of a "block"

diagonal S-matrix,

$$\begin{pmatrix} \uparrow \\ F(+k) \\ B(-k) \\ F(+k') \\ B(-k') \\ \downarrow \end{pmatrix} = \begin{pmatrix} \searrow & & & \\ & S_{+k,+k} \; S_{-k,+k} & & \\ & S_{+k,-k} \; S_{-k,-k} & & \\ & & S_{+k',+k'} \; S_{-k',+k'} & \\ & & S_{+k',-k'} \; S_{-k',-k'} & \\ & & & \searrow \end{pmatrix} \begin{pmatrix} \uparrow \\ A(+k) \\ G(-k) \\ A(+k') \\ G(-k') \\ \downarrow \end{pmatrix}, \qquad (11)$$

where the arrows indicate that $k \in \{-\infty, \infty\}$ and the expansion coefficients $A, B, G,$ and F

represent the Fourier transform of the reactants and products [6]. For simple potentials,

such as a square well, solving the Schrödinger equation in the interaction region is

straightforward and the S-matrix elements can be obtained analytically. More interesting

and realistic potentials however, can become difficult or impossible to solve analytically

and require numerical techniques. Both time dependent and time-independent approaches have been derived to compute S-matrix elements numerically. The Channel Packet Method, a time-dependent approach, is used to compute the S-matrix elements in this thesis.

2.2 The Channel Packet Method

As noted earlier the CPM was developed by Dr. David Weeks and Dr. David Tannor [1-3]. The CPM is a process through which S-Matrix elements are calculated numerically by applying the classical Møller operators (13) to propagate the reactant states $|\Psi_{in}\rangle$ and the product states $|\Psi_{out}\rangle$. The "scattering" equation relates the incoming state with the outgoing state:

$$|\psi_{out}\rangle = \hat{S}|\psi_{in}\rangle,\tag{12}$$

where $\hat{S}$ denotes the "scattering" operator. The CPM formulates the S-matrix elements that make up $\hat{S}$ through a time-dependent correlation function between what are known as Møller states. The Møller states are formed by applying the Møller operators to the reactant and product states.

2.2.1 Møller Operators

The Møller operators are defined as:

$$\Omega_{\pm} = \lim_{t\to\mp\infty}[\exp(iHt/\hbar)\exp(-iH_o t/\hbar)],\tag{13}$$

where H_o and H represent the asymptotic and full Hamiltonians:

$$H_o = \frac{p^2}{2m},\tag{14}$$

and
$$H = \frac{p^2}{2m} + V(x).$$
(15)

The relationship between the full and asymptotic Hamiltonians is defined as:

$$\lim_{x \to \pm\infty} \begin{cases} V(x) \to 0 \\ H = H_o \end{cases}.$$
(16)

The operators are related to the scattering operator by [7]

$$\hat{S} = \Omega^{\dagger}_{-} \Omega_{+}.$$
(17)

The relationship defined by equation 16 requires that the potential go to zero as $x \to \pm\infty$.

The Møller operators act on the reactant and product states to form the Møller states in

the following way:

$$\left| \psi^+ \right\rangle = \Omega_+ \left| \psi_{in} \right\rangle,$$
(18)

and
$$\left| \psi^- \right\rangle = \Omega_- \left| \psi_{out} \right\rangle.$$
(19)

The plus and minus superscripts denote the "reactant" and "product" Møller states

respectively. Numerically applying the Møller operators results in the reactant state

$\left| \Psi_{in} \right\rangle$, being propagated to $t = -\infty$ under the asymptotic Hamiltonian and then propagated

to $t = 0$ under the full Hamiltonian. Conversely, the product state $\left| \Psi_{out} \right\rangle$, is propagated to

$t = \infty$ under the asymptotic Hamiltonian and then propagated to $t = 0$ under the full

Hamiltonian. Numerically speaking, the states cannot be propagated to $t = \pm\infty$, however,

the asymptotic limits are achieved when the states have propagated completely outside

the interaction region [9]. To better understand the application of the Møller operators a

step-by-step discussion is provided below for the specific case of a square well potential.

Figures 2 and 3 show the coordinate and momentum representations of a typical CPM setup. Gaussian wave packets represent the product and reactant states. The coordinate representation of an initial state is defined as:

$$\Psi(x,0) = \frac{1}{\sigma_x^{1/2}(2\pi)^{1/4}} \exp\left[ik_o(x-x_o)\right]\exp\left[-(x-x_o)^2/4\sigma_x^2\right], \qquad (20)$$

where σ_x describes the initial spread in the position of the particle and x_o serves to define the center of the wave packet. The corresponding probability density takes the form of a Gaussian function and is described as:

$$\Psi^*\Psi = \frac{1}{\sigma_x\sqrt{2\pi}} \exp\left[-(x-x_o)^2/2\sigma_x^2\right]. \qquad (21)$$
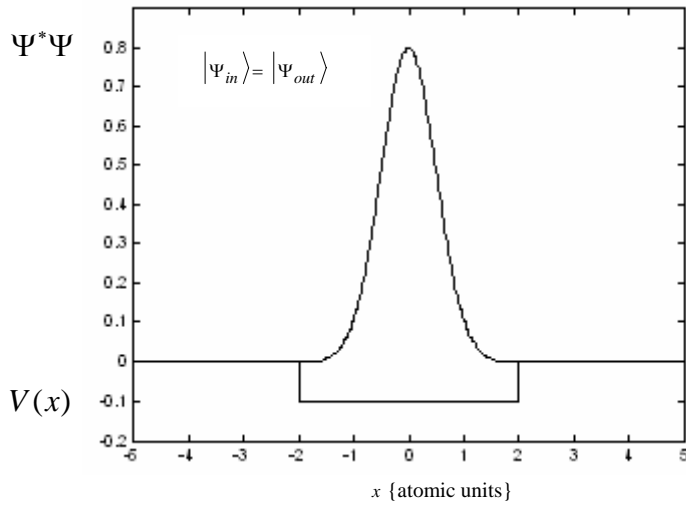
Figure 2. The initial product and reactant Gaussian wave packets $\left|\Psi_{in}\right\rangle$ and $\left|\Psi_{out}\right\rangle$ plotted in the coordinate representation. The square well potential depth is scaled by a factor of 10. The probability density is shown.

$\Psi^*\Psi$

$\left|\Psi_{in}\right\rangle = \left|\Psi_{out}\right\rangle$

k {atomic units}
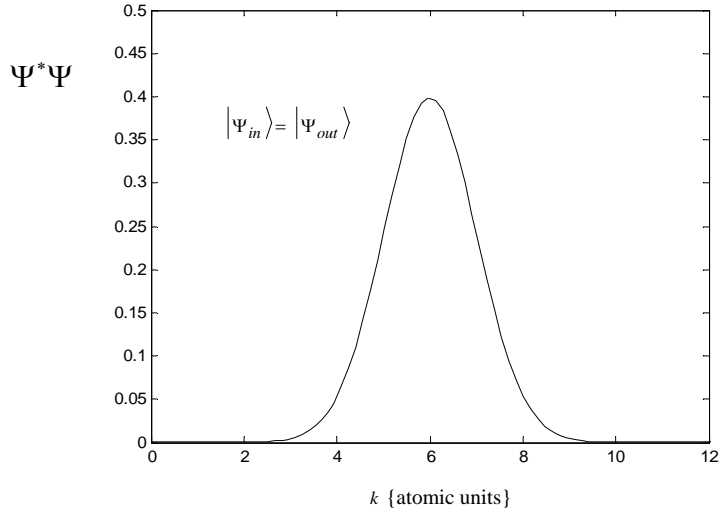
Figure 3. The initial product and reactant Gaussian wave packets $\left|\Psi_{in}\right\rangle$ and $\left|\Psi_{out}\right\rangle$ plotted in the momentum representation. where only $+k$ is considered. The probability density is shown.

The complex modulation $\exp\left[ik_o(x-x_o)\right]$ in equation (20) serves to define the average momentum

$$\left\langle p \right\rangle = \hbar k_o .\qquad(22)$$

The physical interpretation of the state defined by equation (20) is then a particle localized within a spread of σ_x about x_o moving with an average momentum, $\hbar k_o$. The expansion coefficients of the initial states are then computed using the Fourier transform of $\psi(x,0)$:

$$\eta(k) = \frac{1}{\sqrt{2\pi}} \int_{-\infty}^{\infty} \Psi(x,0)\exp(-ikx)dx ,\qquad(23)$$

with the corresponding probability density

$$\left|\eta(k)\right|^2 = \frac{2\sigma_x}{\sqrt{2\pi}}\exp\left[-2\sigma_x^{2}(k_o-k)^2\right].\qquad(24)$$

12

The momentum probability density is thus also a Gaussian centered about k_o with a

spread $\sigma_k = (2\sigma_x)^{-1}$. The product of the uncertainties has its minimum value in the initial

Gaussian wave packet:

$$\sigma_x \sigma_k = \Delta x \Delta p\big|_{Gauss} = \frac{\hbar}{2}.$$

(25)

As discussed earlier the states must be propagated under the asymptotic Hamiltonian

during the construction of the Møller states. Since $V(x) = 0$ in the asymptotic regions, the

states propagate as free particles during the first half of the Møller operators. The

blessing in this is that one can propagate to the asymptotic channels analytically using the

time-dependent, free-particle, Gaussian state [8]:

$$\Psi(x,t) = \frac{\exp\left[i\frac{\tau}{t}\left(\frac{x - x_o}{2\sigma_x}\right)^2\right]\exp\left[\frac{-(i\tau/4t\sigma_x)(x - x_o - \hbar k_o t/m)^2}{1 + it/\tau}\right]}{\sigma_x^{1/2}(2\pi)^{1/4}(1 + it/\tau)^{1/2}},$$

(26)

where,

$$\tau \equiv \frac{2\sigma_x^2 m}{\hbar}.$$

(27)

However, in doing so there is a distortion of the Gaussian states in time. That is, the

initial uncertainty in position, $\sigma_x(t_o)$, becomes larger in time and the wave function

spreads as

$$\sigma_x(t) = \sigma_x(t_o)\left(1 + \frac{t^2\hbar^2}{4m^2\sigma_x(t_o)}\right)^{1/2} \text{ [8].}$$

(28)

13

The spreading can be understood by realizing that the initial Gaussian state is a superposition of plane waves, each having different momentum. Thus, as time progresses the initial uncertainty in position is compounded by the initial uncertainty in the momentum.

The coordinate representation (Figure 2) shows two Gaussian wave packets centered in the middle of a square well potential. The reactant and product states are constructed to be the same in this case. The results of the application of the first part of the Møller operators are shown in Figure 4. The reactant wave packet has propagated backwards in time 300000 atomic units (a.u.) (to the left since it has positive momentum), and the product has propagated forward in time 300000 a.u. (to the right since it too has positive momentum). The propagations are performed analytically using equation (26). These states are defined as the intermediate Møller states

$$\left| \psi_\alpha^\pm \right\rangle = \lim_{t \to \mp\infty} \exp(-iH_o t / \hbar) \left| \Psi_{\substack{in \\ out}} \right\rangle. \tag{29}$$
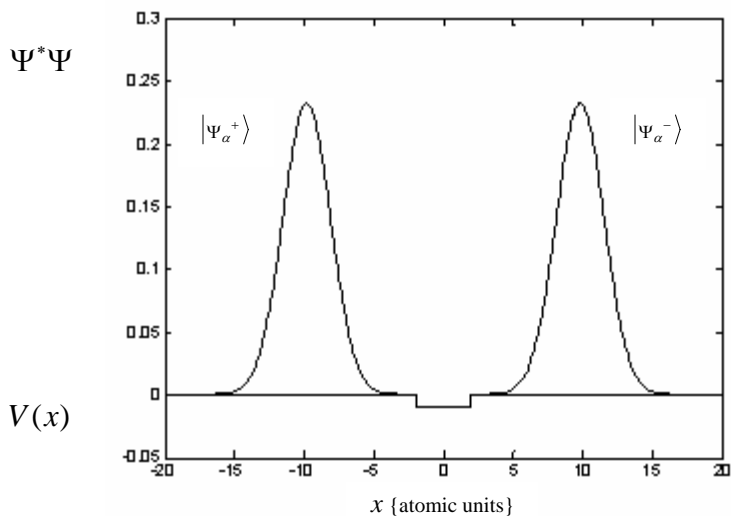
Figure 4. The probability density of the intermediate Møller states, $\left| \Psi_\alpha^+ \right\rangle$ and $\left| \Psi_\alpha^- \right\rangle$ (after $t = 30000\ a.u.$) plotted in the coordinate representation. The square well potential is also plotted.

14

Both propagations have lasted long enough to ensure the wave packets are completely outside the square well. It should be noted that, by construction, these states contained only positive momentum (Figure 3). Therefore, it is a simple matter to analytically propagate the states completely outside the interaction region.

The final step in the construction of the Møller states is to apply the second half of the Møller operators to these intermediate states. This application is mathematically defined as:

$$\left|\psi^{\pm}\right\rangle = \lim_{t \to \mp\infty} \exp(iHt/\hbar)\left|\Psi_{\alpha}^{\pm}\right\rangle \tag{30}$$

where H contains the square well potential (atomic units),

$$V(x) = \begin{cases} -0.01 & -2 \leq x \leq 2 \\ 0 & elsewhere \end{cases} \tag{31}$$

The application of equation (30) is done numerically using the split operator. The result of this application is shown in Figure 5. The states have propagated back to $t = 0$. Since the product and reactant contain only positive momentum, only $S_{+k,+k}$ (the probability of coming in with positive momentum and going out with positive momentum) may be computed. The Møller operators are specific to scattering theory, the choice of propagation method, however, is not. In this thesis the method of propagation is the split-operator method.

2.2.2 The Split Operator Method

The Split Operator is used in the CPM to propagate the initial product and reactant wave functions mentioned in the previous section.

$\Psi^*\Psi$

$V(x)$

x {atomic units}
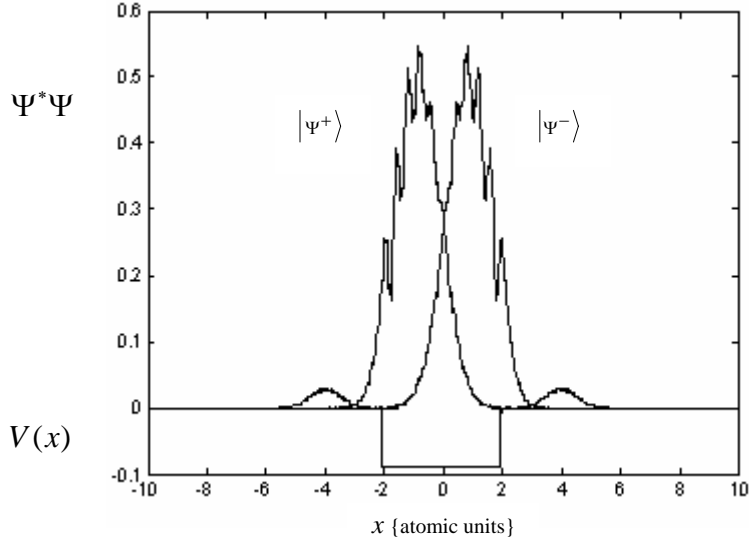
Figure 5. The Møller states, $|\Psi^+\rangle$ and $|\Psi^-\rangle$ plotted in the coordinate representation. The square well potential has been scaled by a factor of 10. The probability density is shown.

The split operator approximates the time evolution operator,

$$\hat{U} = \exp\left[\lambda(\hat{T}+\hat{V})\right] \tag{32}$$

where,

$$\lambda = -i\frac{t}{\hbar} \tag{33}$$

as

$$\hat{U} \approx \exp\left(\lambda\frac{\hat{T}}{2}\right)\exp\left(\lambda\hat{V}\right)\exp\left(\lambda\frac{\hat{T}}{2}\right) + O\left(\Delta t^3\right). \tag{34}$$

The splitting contains an error since the commutator, $[V(x),T] \neq 0$; the error term can be easily obtained from a Taylor expansion of the exponentials (Appendix A). Terms appearing in the split operator are:

16

$$T = \frac{\hbar^2 k_j^{\ 2}}{2m}, \tag{35}$$

$$V(x_j), \tag{36}$$

$$\lambda = -i\frac{t_l}{\hbar}, \tag{37}$$

and
$$j \in \left\{ -\frac{N}{2} : \frac{N}{2} \right\}, \quad t_l \in \left\{ t_{\min} : t_{\max} \right\}. \tag{38}$$

The index j is defined over the set described in equation (38) specifically for the application of using the Fast Fourier Transform (FFTs) where N is the number of grid points. Propagation is achieved by applying the approximate time evolution operator listed in equation (34) to the product and reactant wave packets. Using Fast Fourier Transforms one can rapidly switch between the position and momentum representations of the reactant and product wave packets. The time evolution operator $\hat{U}$ is split into position and momentum dependent parts. The advantage of using the approximate, split operator is that the position and momentum parts of the operator become simple multiplicative factors in the coordinate and momentum representations. The latter point saves computational effort. To explain this point, consider applying the time evolution operator to a Gaussian wave packet $|\Psi(x)\rangle$. In order to characterize the evolving wave packet one would use:

$$\Psi(x_i, t_{i+1}) = \exp\left[\lambda \left(-\frac{\hbar^2}{2m} \frac{\partial}{\partial x^2} + V(x_i) \right) \right] \Psi(x_i, t_i) \tag{39}$$
.

Each time step requires the use of a finite difference method resulting in a substantial

increase in the total computational effort needed to fully propagate the wave packets.

Conversely, with the use of the split operator method, a FFT is applied to $\Psi(x)$ to form

$\Psi(k)$. The differential representation of the momentum operator is avoided, since in the

momentum representation, the operator is diagonal. The process of applying FFT's and

IFFT's (FFT^{-1}) to switch back and forth between the coordinate and momentum

representation continues with a single time step consisting of

$$\Psi(x,t_{i+1}) = IFFT\left[\exp\left(\lambda \frac{\hat{T}}{2} \right) FFT \left[\exp\left(\lambda \hat{V} \right) IFFT \left[\exp\left(\lambda \frac{\hat{T}}{2} \right) FFT \left[\Psi(x,t_i) \right] \right] \right] \right]. \quad (40)$$

The process is continued over and over again until the desired propagation time is

achieved. The application of the split operator is used to propagate the reactant and

product wave packets in all simulations performed in this thesis. The simulations

performed do not account for the error associated with the split operator. However, Δt is

made sufficiently small (1 a.u.) in an effort to make the error negligible.

2.2.3 Computing the S-Matrix Elements

After the Gaussian product and reactant wave packets are formulated and the

Møller states constructed, the S-matrix elements are computed. A convenient starting

point[1] for discussing how we attempt to calculate the S-matrix elements starts with the

Fourier Transform (FT) of the correlation function between the reactant and product

Møller states:

---

[1] For the derivation of this equation see D.E. Weeks and D.J. Tannor, Chem. Phys. Letters 207 (1993) 301.

$$FT\big[C(t)\big]=\int_{-\infty}^{\infty}dt\exp(iEt)C(t)=\frac{2\pi m}{|k|}\times[\eta^{-}(-k)\eta^{+}(+k)\,S_{-k,+k}$$

$$+\eta^{-}(+k)\eta^{+}(+k)\,S_{+k,+k}$$
$$+\eta^{-}(-k)\eta^{+}(-k)\,S_{-k,-k}$$
$$+\eta^{-}(+k)\eta^{+}(-k)\,S_{+k,-k}]$$

(41)

where,

$$C(t)=\left\langle\Psi^{-}\left|\exp(-iHt)\right|\Psi^{+}\right\rangle.$$

(42)

and the plus and minus superscripts in the $\eta^{\pm}$ stand for reactant and product respectfully.

The expansion coefficients $\eta^{\pm}(\pm k)$ listed in equation (41) are the same as those defined

previously in equation (23). The plus and minus designations in the S-matrix elements

stand for the four possible combinations in a scattering model. For example, $S_{-k,+k}$,

would describe the S-matrix element for an incoming state (reactant) having positive

momentum and an outgoing state (product) leaving with negative momentum. The

absolute value of $S_{-k,+k}$ squared would then give the probability for coming in from the

left with positive momentum and leaving to the left with negative momentum. The time-

dependent correlation function of equation (42) is numerically evaluated using the split-

operator by propagating $\left|\Psi^{+}\right\rangle$ using the full Hamiltonian until it is completely outside the

interaction region. At each time step the scalar product given in equation (42) is

computed. It is important to note that in order to completely form the correlation

function one must propagate $\left|\Psi^{+}\right\rangle$ both forward and backward in time until $\left|\Psi^{+}\right\rangle$ is

completely outside the interaction region.

III Application of the CPM

3.1 Previous Technique

Past approaches, such as those described in [1-3], have been to simply invert equation (41) to establish the S- matrix elements,

$$S_{\pm k, \pm k} = \frac{|\hbar||k| FT[C(t)]}{2\pi m \ \eta^-(\pm k)\eta^+(\pm k)}.$$ (43)

In order to write equation (43) specific requirements must be imposed on the product and reactant states. That is, the product and reactant Gaussian wave packets must contain only positive or negative momentum ranges. For example, if one wishes to compute the S-matrix element $S_{+k, +k}$, the reactant and product wave packets must contain only positive momentum ranges (Figure 3). Equation (41) then simplifies to

$$S_{+k, +k} = \frac{|\hbar||k| FT[C(t)]}{2\pi m \ \eta^-(+k)\eta^+(+k)},$$ (44)

since the $\eta^-(-k)$ and $\eta^+(-k)$ terms all go to zero. Similarly, the other S-matrix elements may be computed under the guidelines given in table 1. Weeks and Tannor developed this method to formulate S-matrix elements with excellent results. The limitation in using there approach however, was that the product and reactants could only contain either positive or negative momentum. As a result they could not accurately calculate S-matrix elements near zero energy.

The explanation why previous attempts failed to produce good results at low energies is that there was not enough information contained in the initial wave packets.

Table 1. S-matrix selection table.

To Compute	S_{+k+k}	S_{+k-k}	S_{-k+k}	S_{-k-k}
Use $\eta^-(k)=0$	$k<0$	$k>0$	$k<0$	$k>0$
$\eta^+(k)=0$	$k<0$	$k<0$	$k>0$	$k>0$
And divide $FT\big[C(t)\big]$ by	$\eta^-(+k)\eta^+(+k)$	$\eta^-(+k)\eta^+(-k)$	$\eta^-(-k)\eta^+(+k)$	$\eta^-(-k)\eta^+(-k)$

The requirement that the reactant and product states contain only positive or negative momentum leads to a loss of information at low energies. Consider the product and reactant states shown in Figure 3. The wave packets are centered about $k_o = 6$. Notice that the probability density near the low momentum ranges is effectively zero. Of course, the theoretical wave packet extends to plus and minus infinity, and thus would be fully represented across the entire momentum range. However, computers are limited in storing very small numbers and thus the amplitude in the low momentum range is interpreted as zero; leading to a loss of information for approximately $k \leq 1$. It should be noted as well that another loss of information is incurred for approximately $k \geq 11$. The obvious solution is to center the wave packets closer to zero.

Consider the wave packet shown in Figure 6. Notice that there is a substantial probability density near low momentum. However, as the center of the wave packets are moved into the low momentum regime the wave packets overlap zero and exhibit

substantial amplitude in the negative momentum regime. The requirement that the

product and reactant wave packets contain only positive or negative momentum ranges is

violated.
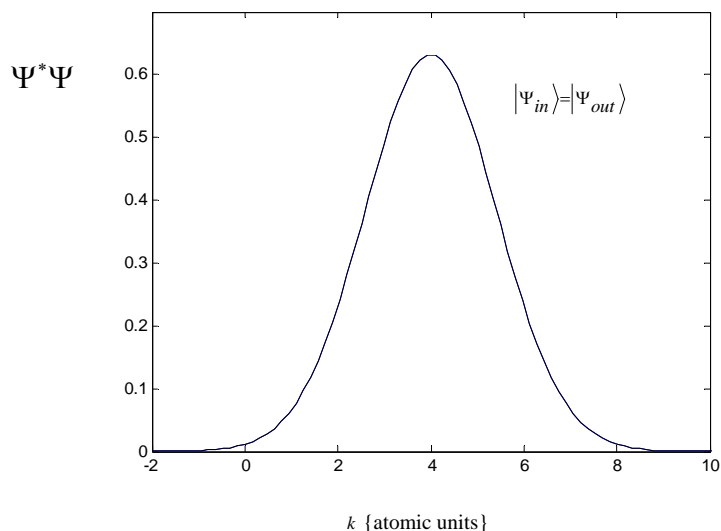
Figure 6. Initial product and reactant Gaussian wave packets plotted in the momentum representation showing overlap. The probability density is shown.

Previously, Weeks and Tannor simply ignored the overlapping amplitude and proceeded

with equation (43) under the formulations made in Table 1. In an effort to reduce the

error associated with neglecting the overlapping momentum amplitude they centered the

wave packet such that there was as little overlap as possible. However, this becomes

problematic since one must carefully construct the wave packets such that the tails go to

zero at $k = 0$. In doing so however, one is always fighting the battle of having the tails go

to zero while still needing information to be numerically stored at low energies.

A new problem is introduced if the reactant or product state has both positive and

negative momentum. Imagine applying the Møller operator Ω_+ to a reactant state centered

in the middle of a potential well like that of Figure 1 with a momentum representation

22

like that of Figure 6. As the wave packet is propagated backwards in time under the asymptotic Hamiltonian, most of the wave packet will move to the left, however some would move to the right since it contains some negative momentum. The time required to fully propagate the reactant and product wave packets completely outside the interaction region increases due to movement in both directions.

The subsequent increase in propagation time will require a larger grid since, according to according to equation (28), the wave packet will spread as a function of time. Since Weeks and Tannor used wave packets with all positive or negative momentum ranges this problem was avoided; it is fairly easy to propagate the wave packets outside the interaction region when they only contain positive or negative momentum. In order to apply the CPM to wave packets in the low energy regime one must reformulate the previous application and loosen the restriction that the product and reactant wave packets contain only positive or negative momentum.

3.2   New Technique

In order to establish enough information in the low energy regime, one formulates the product and reactant wave packets to have both positive and negative momentum. In doing so however, the requirements allowing the use of equation (43) are violated. Therefore, a new approach must be applied to the CPM to handle the calculation of S-matrix elements at low energy. The algorithm developed in this thesis extends equation (41) into a matrix formulation with four product and reactant wave packets. The mathematical matrix equivalent is

$$\begin{pmatrix} FT[C(t)_1] \\ FT[C(t)_2] \\ FT[C(t)_3] \\ FT[C(t)_4] \end{pmatrix} = \frac{2\pi m}{|k|} \left(\eta\right) \begin{pmatrix} S_{-k,+k} \\ S_{+k,+k} \\ S_{-k,-k} \\ S_{+k,-k} \end{pmatrix}, \tag{45}$$

where the η-matrix is given by,

$$\eta = \begin{pmatrix} \eta^-(-k)_1\eta^+(+k)_1 & \eta^-(+k)_1\eta^+(+k)_1 & \eta^-(-k)_1\eta^+(-k)_1 & \eta^-(+k)_1\eta^+(-k)_1 \\ \eta^-(-k)_2\eta^+(+k)_2 & \eta^-(+k)_2\eta^+(+k)_2 & \eta^-(-k)_2\eta^+(-k)_2 & \eta^-(+k)_2\eta^+(-k)_2 \\ \eta^-(-k)_3\eta^+(+k)_3 & \eta^-(+k)_3\eta^+(+k)_3 & \eta^-(-k)_3\eta^+(-k)_3 & \eta^-(+k)_3\eta^+(-k)_3 \\ \eta^-(-k)_4\eta^+(+k)_4 & \eta^-(+k)_4\eta^+(+k)_4 & \eta^-(-k)_4\eta^+(-k)_4 & \eta^-(+k)_4\eta^+(-k)_4 \end{pmatrix}. \tag{46}$$

Using a four-by-four matrix approach one is able to handle product and reactant wave packets containing any combination of positive and negative momentum. The entire S-matrix is then computed by inverting equation (45):

$$\begin{pmatrix} S_{-k,+k} \\ S_{+k,+k} \\ S_{-k,-k} \\ S_{+k,-k} \end{pmatrix} = \frac{|k|}{2\pi m} \eta^{-1} \begin{pmatrix} FT[C(t)_1] \\ FT[C(t)_2] \\ FT[C(t)_3] \\ FT[C(t)_4] \end{pmatrix}. \tag{47}$$

In the limit that the product and reactant wave packets are constructed to have only positive or negative momentum, the η-matrix defined by equation (46) becomes diagonal, and reduces to the four independent S-matrix equations of (43).

The requirement of equation (47) is that the inverse of η must exist. Therefore, a necessary condition is that the η-matrix must have a non-zero determinant. Numerically representing a Gaussian wave packet will always lead to expansion coefficients that are interpreted as zero near the tail end of the wave packet. In turn, the η-matrix will be filled with zeros and therefore become singular. However, as in previous approaches, this

24

is simply interpreted as an inability to extract information from the tail ends of the product and reactant wave packets. Therefore, η need only to be non-singular in the energy range of interest.

Due to the nature of a four-by four matrix approach one must formulate four separate product and reactant states. One could simply establish four wave packets centered at four distinct momentum values. In doing so, one would ensure the η-matrix is non-singular in the energy range of interest. In turn, four propagations would be needed to formulate the four transforms listed in equation (47). However, if one is careful in their construction of the product and reactant states, only two propagations are required. To explain, consider formulating the product and reactant wave packets in the following way. Establish two Gaussian wave packets, one centered about k_o and the other about $-k_o$. Reactant 1 is made to be the same as product 1 and product 2 the same as reactant 1. The choice of where to put the wave packets in the coordinate representation is arbitrary. The setup is shown in Figures 7 and 8.

Given the initial setup described above one then numerically computes the corresponding Møller states for each product and reactant. Four correlation functions are then computed to establish the right hand side of equation (47). Given the setup described above, the four correlation functions would be

$$C_1(t) = \left\langle \Psi^-_{\,2} \left| \exp(-iHt) \right| \Psi^+_{\,1} \right\rangle$$

$$C_2(t) = \left\langle \Psi^-_{\,1} \left| \exp(-iHt) \right| \Psi^+_{\,1} \right\rangle$$

$$C_3(t) = \left\langle \Psi^-_{\,1} \left| \exp(-iHt) \right| \Psi^+_{\,2} \right\rangle \tag{48}$$

$$C_4(t) = \left\langle \Psi^-_{\,2} \left| \exp(-iHt) \right| \Psi^+_{\,2} \right\rangle .$$
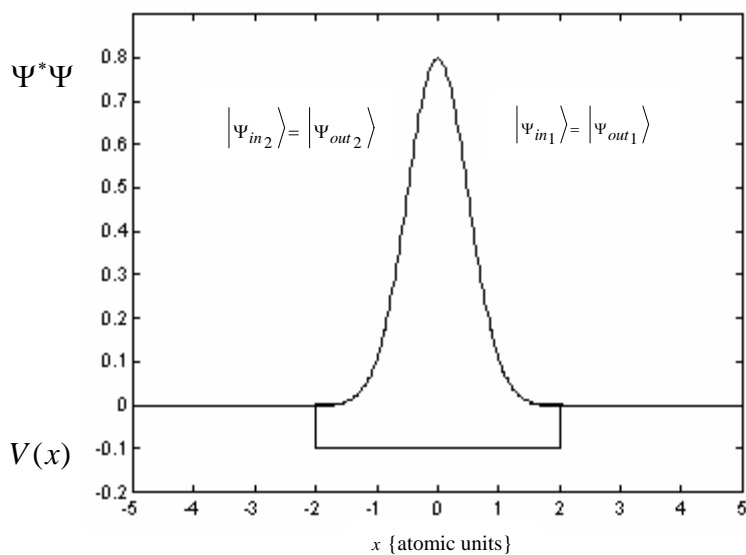
Figure 7. Initial product and reactant Gaussian wave packets $\left| \Psi_{out_1 \atop 2} \right\rangle$ and $\left| \Psi_{in_1 \atop 2} \right\rangle$ plotted in the coordinate representation. The square well potential has been scaled by a factor of 10. The probability density is shown.
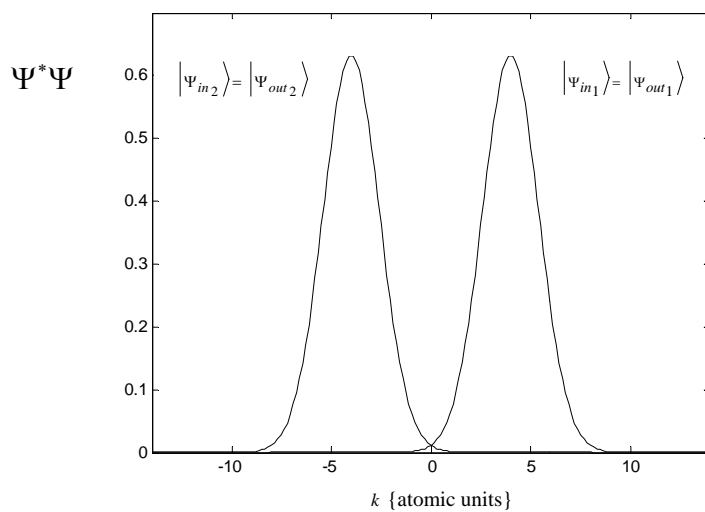
Figure 8. Initial product and reactant Gaussian wave packets $\left| \Psi_{out_1 \atop 2} \right\rangle$ and $\left| \Psi_{in_1 \atop 2} \right\rangle$ plotted in the momentum representation. The probability density is shown.

26

Once the correlation functions are computed a simple Fourier transform is performed and the S-matrix is determined using equation (47).

3.2.1 Summary of Steps for New Approach

A summary of the steps used to perform a simulation is listed below.

1. Make product 1 and reactant 1 equal to one another and contain nearly all positive momentum.

2. Make product 2 and reactant 2 equal to one another and contain nearly all negative momentum.

3. Using equation (23) fill in the η-matrix based on the product and reactant wave packets from steps 1 and 2 as shown below. The subscripts 1 and 2 represent reactant and product one and two.

$$\eta = \begin{pmatrix} \eta^-(-k)_2\eta^+(+k)_1 & \eta^-(+k)_2\eta^+(+k)_1 & \eta^-(-k)_2\eta^+(-k)_1 & \eta^-(+k)_2\eta^+(-k)_1 \\ \eta^-(-k)_1\eta^+(+k)_1 & \eta^-(+k)_1\eta^+(+k)_1 & \eta^-(-k)_1\eta^+(-k)_1 & \eta^-(+k)_1\eta^+(-k)_1 \\ \eta^-(-k)_1\eta^+(+k)_2 & \eta^-(+k)_1\eta^+(+k)_2 & \eta^-(-k)_1\eta^+(-k)_2 & \eta^-(+k)_1\eta^+(-k)_2 \\ \eta^-(-k)_2\eta^+(+k)_2 & \eta^-(+k)_2\eta^+(+k)_2 & \eta^-(-k)_2\eta^+(-k)_2 & \eta^-(+k)_2\eta^+(-k)_2 \end{pmatrix}$$

4. Apply the split operator to numerically compute the Møller states for each product and reactant under the operations defined in equations (18) and (19).

5. Use the split operator to propagate the reactant Møller states both forward and backward in time under the full Hamiltonian while computing the correlation functions defined by equation (48) at each time step.

6. Compute the Fourier transforms to convert the time dependent correlation functions into to the energy representations listed on the right hand side of equation (47).

7. Finally use equation (47) to compute the S-matrix elements.

Using the algorithm described above one can completely characterize wave packets containing both negative and positive momentum ranges. By keeping the full η-matrix information can be stored in the low energy regime; thus improving the calculations of the S-matrix elements across the entire energy spectrum. Furthermore, the method used is more complete than previous methods since it does not require reactant and product states having all positive or negative momentum.

3.2.2 An Interesting Implication of the New Approach

It should be noted that aside from the full matrix approach to the CPM there is an interesting difference between equations (47) and (43). Equation (47) implies that when reactant and product states contain both positive and negative momentum, one cannot know one S-matrix element without simultaneously knowing the other three. That is, there is an inter relationship among the S-matrix elements. Equation (43) requires no connection whatsoever between the different S-matrix elements except that the sum of the transmission and reflection coefficients be one. Furthermore, in the limit that the product and reactant wave packets contain only positive or negative momentum ranges, the η-matrix becomes diagonal and the S-matrix elements become "detangled."

IV   Choice of Parameters

There are several parameters relevant to the CPM. These parameters include: the grid spacings $\Delta x, \Delta k, \Delta t,$ and ΔE, the centering x_o and k_o of the Gaussian product and reactant wave packets, the maximum and minimum values of the grid sizes $x_{\min}^{\max}$, $k_{\min}^{\max}$, and $t_{\min}^{\max}$, the width of the coordinate and momentum wave packets σ_x and σ_k, as well as the number of grid points N. Many of the parameters mentioned are determined using knowledge about the setup of the scattering problem itself. The parameter x_o is somewhat arbitrary, and in the simulations performed in this thesis, was chosen to be the origin. The centering of the momentum wave packet however, has a much more profound effect. The parameters k_o and σ_k will specify the range of energy for which S-matrix elements can be computed. Due to the nature of this thesis, this parameter is chosen such that the momentum representation contains both positive and negative momentum. The product and reactant Gaussian states described in equation (20) require a specification for the initial width of the wave packet. One thing to consider in choosing the parameter σ_x is that the smaller it is the wider the wave packet becomes in the momentum representation. A wide momentum wave packet corresponds to the ability to calculate S-matrix elements over a wide range of energies during a given simulation. However, the wider the wave packet becomes the bigger the grid size needed to fully represent it.

Perhaps the most important computational parameter is N. Since FFT's are used to propagate the wave packets this parameter must satisfy

$$N = 2^n, n \in \{1, 2, 3...\}. \tag{49}$$

29

As the number of grid points is increased more computational effort is needed to perform each FFT. Once N is specified the grid spacing Δx is computed using:

$$\Delta x = \frac{x_{max} - x_{min}}{N}.$$ (50)

The parameters x_{max} and x_{min} are determined by considering the grid size needed to accurately represent all states during the simulation. The intermediate Møller states, like those shown in Figure 4, define the states for which the wave packets are as wide and as far out as any state during a simulation. Hence, they can be used as limiting cases in determining the required coordinate grid size. A further consideration, specific to a square well, is to ensure that Δx is made small enough such that the discontinuities associated with the potential are sufficiently represented. To illustrate this point consider the two potentials shown in Figure 9. These diagrams are meant to show the effect of decreasing the coordinate grid spacing. A large Δx results in a more trapezoidal figure. Thus, in an effort to represent the square well one must ensure the coordinate grid spacing is sufficiently small.
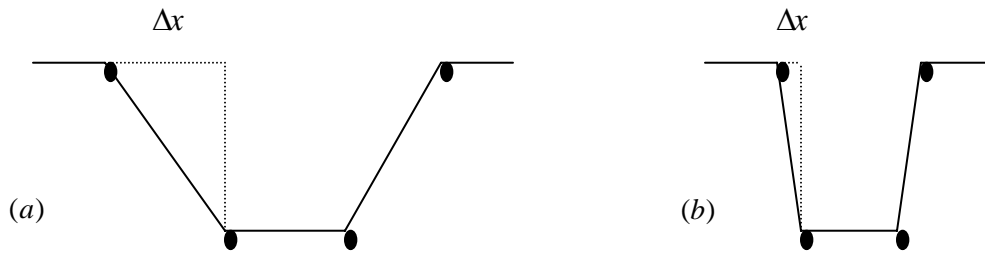
Figure 9. (a) Approximate square well potential for large Δx. (b) Approximate potential showing the convergence to an accurate square well as Δx is decreased.

Since FFTs are used to switch back and forth between the coordinate and momentum representations, the momentum grid spacing is determined by a characteristic of the FFT. The FFT requires a special relationship between the functions transformed from one representation to the other. The relationship is

$$\Delta k = \frac{2\pi}{N\Delta x}.$$ (51)

The parameters k_{max} and k_{min} naturally follow as

$$\left| k_{\substack{max \\ min}} \right| = \frac{N}{2}\Delta k ,$$ (52)

where

$$k_j = j\Delta k, \ j \in \left\{ -\frac{N}{2} : \frac{N}{2} \right\}.$$ (53)

The size of the momentum grid must be able to sustain the momentum wave packets during the entire simulation. A good estimate for ensuring that the momentum representations will be defined throughout the entire simulation is to perform a quick estimate of the maximum value of momentum achieved in the simulation. If one adds the approximate energy gained from the well to the maximum kinetic energy associated with the initial Gaussian wave packet, an approximate value of the maximum momentum can be determined using $k_{max} \approx \left(2mE_{max} \right)^{1/2}$. As long as k_{max} is greater than the computed value the momentum wave packet will be accurately represented throughout the entire simulation.

The parameter Δt is important in the error associated with the Split-Operator method. The larger the time step the less time required to propagate the wave packets but

the greater the error associated with the split operator. As noted in Appendix A, a good

rule of thumb is to ensure the following relationship holds:

$$E_{\max}\Delta t \ll 1, \tag{54}$$

where $E_{\max}$ is computed by adding the largest kinetic energy associated with the initial

Gaussian wave packet to the depth of the well. If equation (54) is maintained the error

associated with the time step is negligible and the split-operator will remain stable.

The propagation times $t_{\min\atop\max}$, should be chosen to ensure that the Møller states are

fully formed, and that the time dependent correlation functions described in equation (48)

start at zero, gradually increase as the Møller states overlap, and then go back to zero.

The energy spacing of the energy grid is completely characterized by the momentum and

the mass of the particle and is represented as

$$\Delta E = \frac{\hbar^2 k_j^2}{2m}. \tag{55}$$

The spacing of the energy grid is not uniform. Although a Fourier transform is

performed to convert the time dependent correlation functions into energy

representations, the requirement that the spacing be uniform is only required for a FFT.

It is important to understand that there is no perfect guide to choosing parameters

in the CPM. The relationships described above are meant to serve as a guide in

formulating the algorithm. An example of the parameters used to perform the simulations

in this thesis is provided in Appendix C. The goal is to define parameters which decrease

propagation time, minimize grid size, and accurately represent the wave functions

throughout the simulation.

32

V   Properties of the New Algorithm

5.1   Verifying the New Approach

Several evaluations were performed throughout this thesis using the new application of the CPM. An initial simulation was performed using product and reactant states having only positive or negative momentum. The η-matrix of equation (46) is diagonal in this case. A square well was used for this simulation and is described by equation (31). The momentum representations of the initial product and reactant wave packets were centered about $k_o = \pm 6$, similar to that shown in Figure 3. The purpose of this simulation was to prove that the new algorithm produced results consistent with previous applications. Figure 10 shows the results of the correlation functions (real part) defined by equation (48). Notice that, as mentioned previously, the correlation functions start at zero and end at zero.
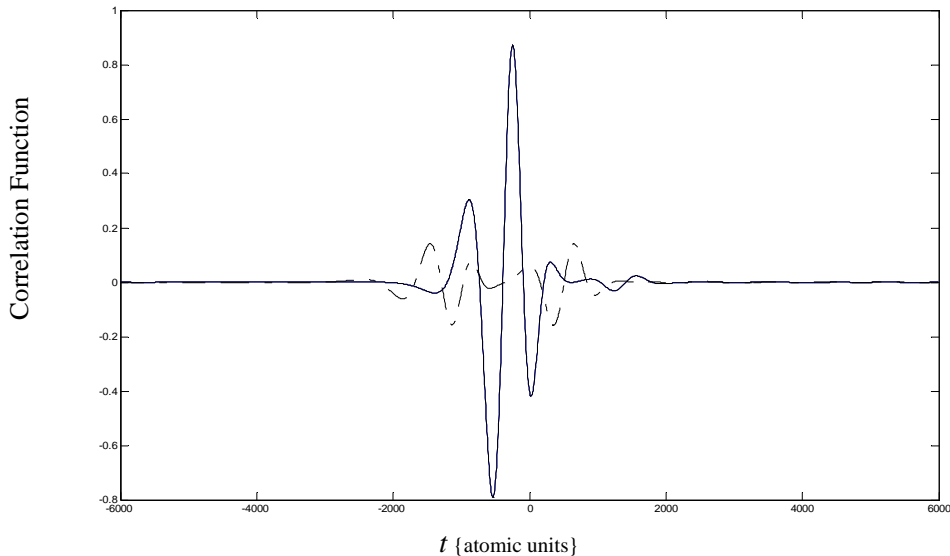
Figure 10. Real part of the correlation functions for simulation 1. The dashed function represents $C_1(t)=C_3(t)$, while the solid line represents $C_2(t) = C_4(t)$.

33
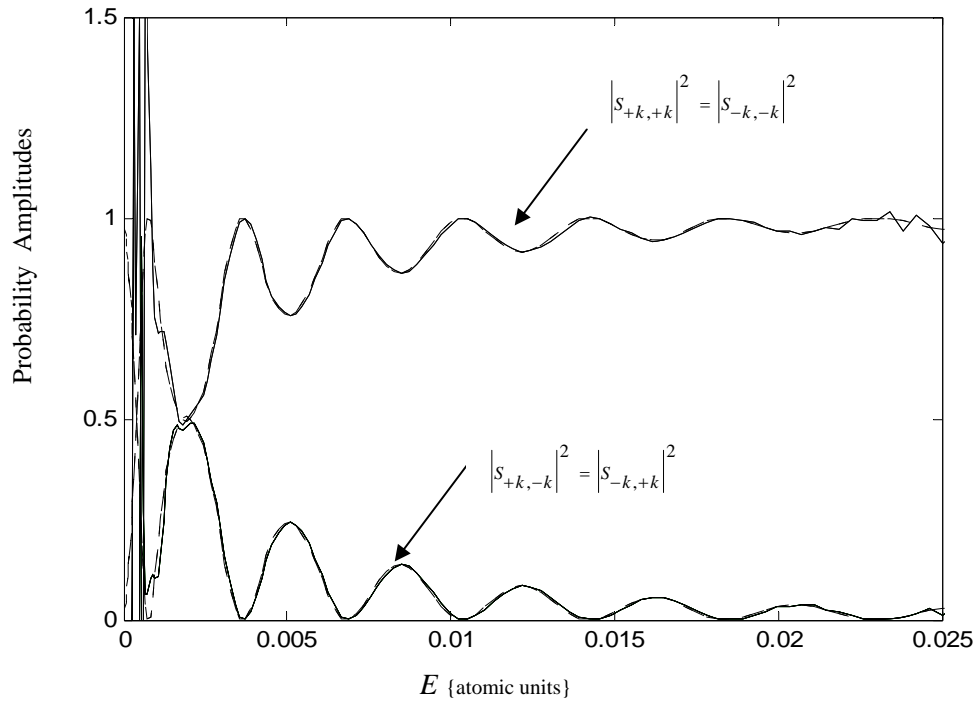
Figure 11. Transmission (upper) and reflection (lower) curves for the square well of depth $V_o = -0.01 \ a.u$. and length $2a = 4$. The dashed lines represent the analytic solutions while the solid lines indicate the numerical results.

As shown by Figure 3, the wave amplitudes are effectively non zero for the momentum range from 3 to 9 a.u. Since the other wave packets were centered about $k_o = -6$ the corresponding amplitudes were non zero for the momentum range from -3 to -9 a.u. Using the mass of the particle, 1833.35 a.u., to convert the momentum range to an energy range, one would expect good results from approximately 0.0025 to 0.022 a.u.

The transmission and reflection curves are shown in Figure 11 along with the analytic solution for a square well. Notice that the results begin to deviate at approximately the energy limits given above. The deviations underscore the limitation that only S-matrix elements corresponding to the range of momentum for which the wave packet is non zero are obtainable. After verifying the algorithm worked correctly we

34

began investigating scattering models for which the product and reactant wave packets

contained a significant amplitude for both positive and negative momentum ranges.

5.2   Low-Energy Scattering (Square Well)

5.2.1   Difficulty in Constructing the Møller States

The focus of the thesis is to investigate scattering when both positive and negative

momentum exist in the product and reactant states. As such the setups depicted in Figures

7 and 8 were used to investigate low energy scattering. Figure 8 shows a small overlap of

negative and positive momentum for the products and reactants. Preliminary calculations

revealed that constructing the Møller states would be problematic. The trouble is that

when positive and negative momentum is present the wave packets spread in both

directions. For example, consider attempting to form the intermediate Møller state for

product1, $\left| \Psi_{out1} \right\rangle$, shown in Figure 8 . As the wave packet is propagated forwards in time

under H_o most of it will move to the right leaving the interaction region. However, a

portion will also move to the left since it also contains negative momentum. Movement in

both directions makes it very difficult to have the wave packets completely leave the

interaction region and thus accurately form the Møller states. Consider Figure 12.

The figure shows the resulting wave packets of Figures 7 and 8 after attempting to

construct the intermediate Møller states. The interaction region again is the square well

described in equation (31). The states were propagated for 800000 atomic units and yet

portions of the wave packets still remain within the square well region (see Figure 12b).

Another important feature of Figure (12) is the size of the coordinate grid needed to

represent the wave packets.
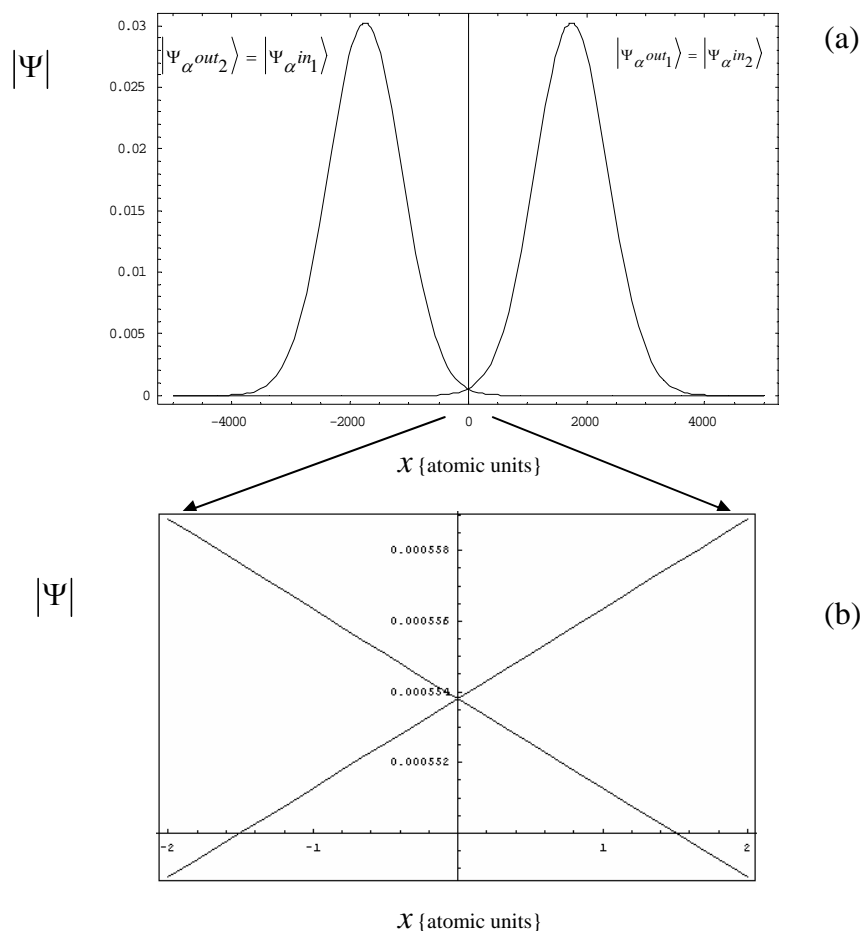
Figure 12. (a) Approximate Møller states after $t = \pm 800000$ ($a.u.$) propagation time. Notice that the wave functions have spread dramatically . (b) Zoomed in portion of interaction region $-2 \leq x \leq 2$.

When the wave packets are constructed to have only positive or negative momentum a grid size of only 40 a.u. is needed to construct the intermediate Møller states (see Figure 4). However, when the reactants and products contain an overlap of negative and positive momentum as shown in Figure 8 the grid size grows to 10000 a.u. and the wave packets are still not completely outside the interaction region. According to equation (50) the larger grid then requires a larger N value, since in order to model a

36

square well, Δx must be very small (see Figure 9). The larger N value makes computation difficult since the simulation times get very large. Despite these drawbacks, an attempt was made at calculating the S-matrix elements using the approximate intermediate Møller states shown in Figure 12.

5.2.2   Approximate Square Well Results

The simulation was performed under the setup described in Figures 7 and 8 using the approximate intermediate Møller states shown in Figure 12. In an effort to have the computation time reasonable N was chosen to be 2^{16} for this simulation. In order to represent the intermediate Møller states of Figure 12 a grid size of 12000 atomic units was chosen leading to a $\Delta x \approx 0.183$ (see equation 50). The large coordinate grid spacing results in the trapezoidal potential function shown in Figure 13. The true square well of equation (31) is shown in the figure for comparative purposes.
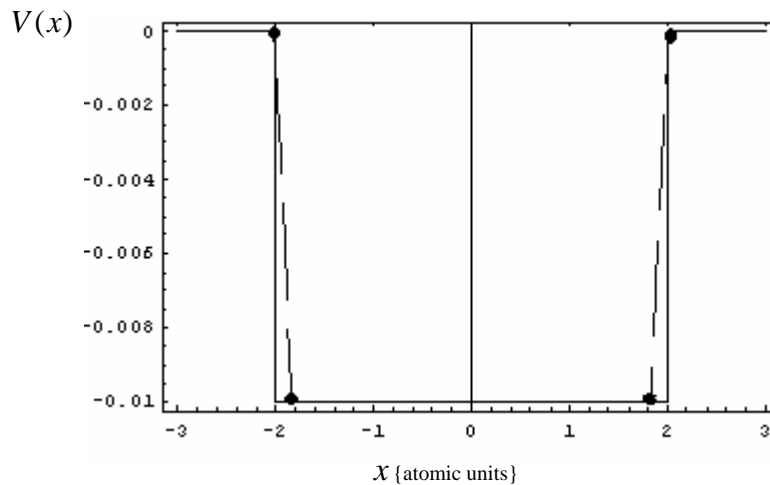
Figure 13. Approximate square well (dashed) and square well (solid) for
$$V(x) = \begin{cases} -0.01 & -2 \le x \le 2 \\ 0 & elsewhere \end{cases}$$
.

It is evident that the results will contain error since the potential function is not exactly a square well. The labeled points demonstrate the discreteness of the numerical potential. In fact, the computer is representing a trapezoidal potential well with linear regions joined by the two labeled points. However, based on Figure 13 the two potential functions are reasonably close and so one would not expect to see an extremely bad fit. The results of the simulation are shown in Figure 14. Notice that the simulated results appear shifted from the analytic solution due to the error in the potential. The other distinct feature is that at low energies the simulated results begin to oscillate. Based on previous calculations it seems reasonable to assume that if Δx was made small enough the curves would line up and thus on can say that the oscillations appear to ring about the analytic values. One should pay careful attention that the behavior at low energies here is much different from results where the reactant and product wave packets contained only positive or negative momentum. The simulated results are oscillating about the known values rather than diverging as shown in Figure 11.

The other interesting property is that $S_{+k,+k}$ and $S_{-k,-k}$ curves oscillate less than the $S_{+k,-k}$ and $S_{-k,+k}$ curves. The reflection coefficient approaches one at low energies while the transmission function goes to zero. The empirical observation then is that the amplitude of the oscillations near low energy depends on the magnitude of the correct value when approximate Møller states are used. In order to perform an error analysis showing that the oscillations diminish and the results converge to the square well solutions one would propagate the reactant and products for longer times in constructing the Møller states.

(a)

(b)
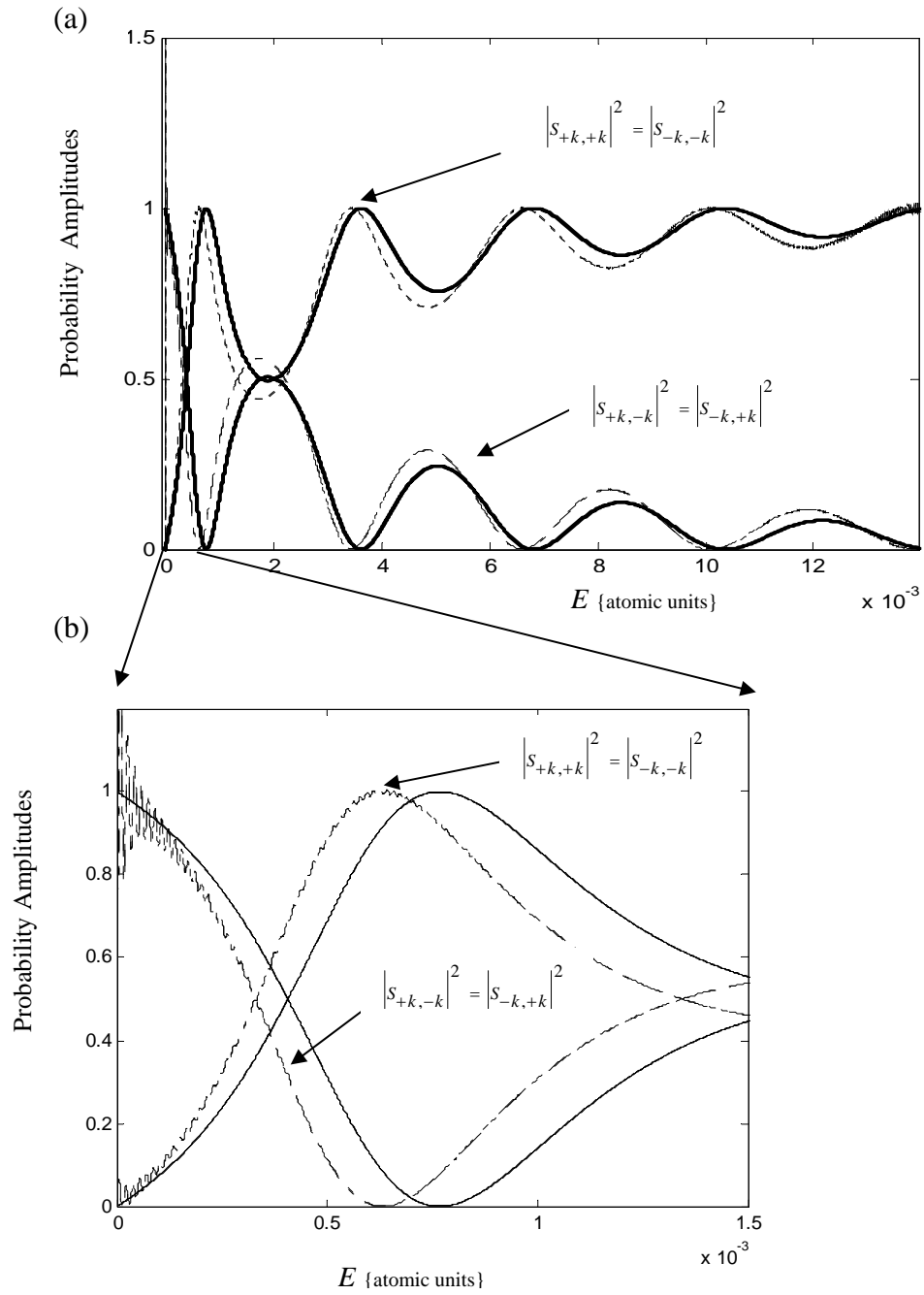
Figure 14. (a) Transmission [$S_{+k,+k}$, $S_{-k,-k}$] and reflection[$S_{+k,-k}$, $S_{-k,+k}$] curves for the square well of depth $V_o = -0.01 \ a.u$. and length $2a = 4$. The analytic solution s are (solid) while the simulated results are (dashed). (b) Zoomed in portion of low energy region showing oscillatory behavior.

The longer the reactants and products are propagated the further they move outside the interaction region and thus the closer one gets in obtaining the correct Møller states. Provided Δx is made small enough, a plot of error vs. the time the wave packets are propagated away from the interaction region should reveal convergence. To perform the analysis one must first establish a measure of convergence for Δx in order to understand just how small the coordinate grid spacing needs to be to approximate the analytic solution of the square well.

5.2.3   Convergence to Square Well based on Δx

In order to establish the convergence of the algorithm four tests where performed at different values of Δx while holding all other parameters constant. The relative error was computed for each of the four simulations based on the theoretical transmission coefficient for a square well. The setup depicted in Figures 2 and 3 was used to perform these tests. A plot of the relative error from a sample test is provided in Figure 15. Measurements were taken at a "low" energy value since this thesis is primarily concerned with low energy scattering.
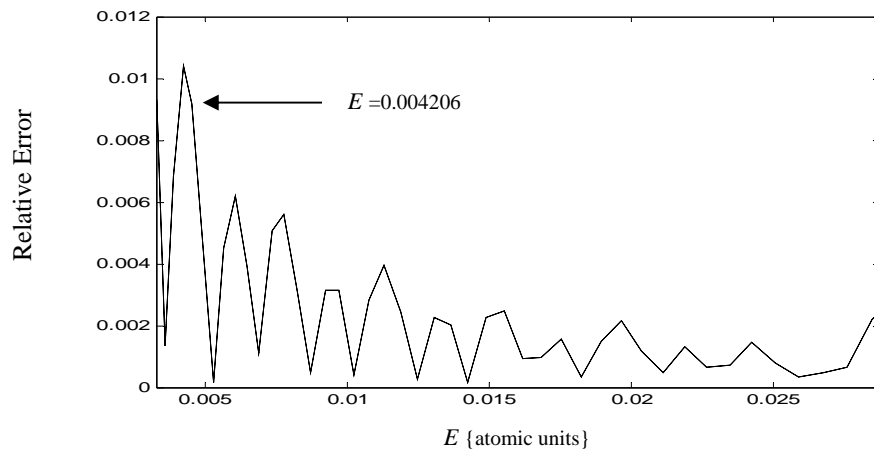
Figure 15. Relative error vs. Energy for sample test for square well of depth $V(x) = -0.01(a.u.)$ and width $2a = 4$. The energy values of the measured data point is labeled.
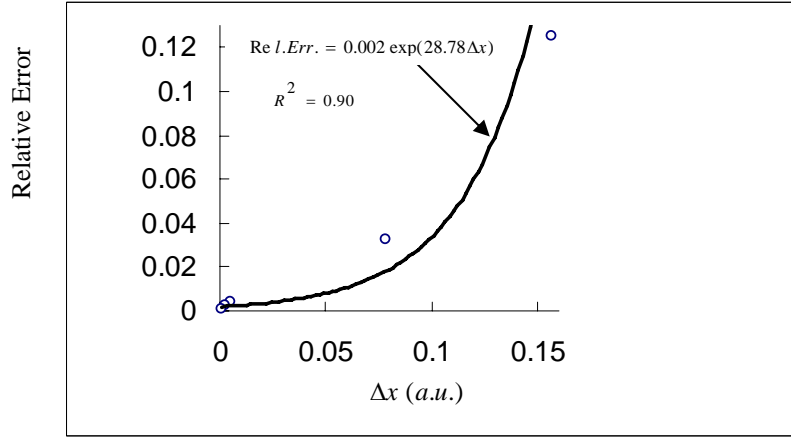
Figure 16. Relative error vs. Δx for square well of depth $V(x)=-0.01(a.u.)$ and width $2a = 4$. An approximate fit reveals that the error exponentially increases as the coordinate grid spacing is increased.

Notice that the relative error approaches small values as Δx is decreased. The resultant fit gives one an idea of the necessary Δx required to accurately represent the square well. It should be noted that even for very small Δx values there is still some relative error. The explanation for this is that, as discussed previously there is error associated with Δt. According to Appendix A, the error term associated with Δt goes like

$$\frac{\left(E_{max}\Delta t\right)^2}{2} \tag{56}$$

where $E_{max} = Vo + \dfrac{k_{max}^{\;2}}{2m}$. For this case $k_{max} \approx 11$, $\Delta t = 1, V_o = 0.01$ and $m = 1833.35$, which lead to an error term of approximately 0.001; in good agreement with the fit of Figure 16 showing that the error goes to 0.0019 as $\Delta x \to 0$.

According to Figure 16, a relative error of approximately 0.5% requires a $\Delta x \approx 0.033$. With the grid size used in the discussion of section 5.2.2 , 12000 a.u., the number of grid points needed to achieve a $\Delta x \approx 0.033$ would be 2^{19}. When the wave

41

packets contain only positive or negative momentum the grid size is only 40 a.u (see

Figure 4), and requires $N = 2^{12}$ to achieve the same grid spacing. Therefore, compared to

considering wave packets that contain only positive or negative momentum to those

which contain both, the number of grid points needed to accurately represent the square

well to within 0.5% relative error increases by a factor of 2^7. As mentioned previously,

the parameter N is important in considering the time required to perform a simulation.

The number of computations for each FFT goes as $N \log N$. Therefore, as a practical

issue it is beneficial to use a low N value in order to keep the simulation times

reasonable.

VI   Square Well Error Analysis

6.1   Methodology

The results of section 5.2.2 showed that an error analysis of the observed "ringing" was needed to show that the simulated results converged to the correct values. Using the parameters $N = 2^{16}$ and $\Delta x \approx 0.183$, we decided to compare several tests, each consisting of larger $t_{\max}^{\min}$. The longer the products and reactants are propagated into the asymptotic channels the closer they get to completely leaving the well, and hence converging to the correct Møller states. The problem, however, was that it was unclear as to what the "real" solution was for a large Δx and thus there was no baseline solution to compare the results. The reader should be reminded of the difficulty in formulating a solution when Δx is large (see Figure 13). At large Δx the discrete representation of the potential takes on a trapezoidal form. An estimated relative error using the parameters $N = 2^{16}$ and $\Delta x \approx 0.183$ was calculated to be approximately 37% based on Figure 16. Therefore, comparing the results to the analytic square well of equation (31) would be computationally prohibitive. Having a baseline solution is desired, however it is not necessary to show the convergence of the computed S-matrix elements.

Previous plots in this thesis (such as Figure 11) have demonstrated that if Δx is made small enough the simulated results converge to the correct solution up to a certain point at very low energy. Since Figure 14 showed that the results "behaved" like the analytic solution across the entire energy range it was no longer a concern to make Δx very small. Relaxing the requirement of small Δx allowed me to explore the effects

43

of increasing t_{max}^{min} without having to have unreasonably long simulation times. The

"ringing" phenomenon seen in Figure 14 is not dependent on Δx but caused primarily by

the intermediate Møller states not clearing the interaction region[2]. While an analytic

solution is desired, it is not needed to show that the amplitude of the oscillations at low

energy converge to zero. The wave packet residual left within the interaction region is

decreased by propagating the reactant and product wave packets for longer times.

Therefore, as t_{max}^{min} is increased the portions of the wave packet left within the well

diminishes and the closer the states become to the correct intermediate Møller states. The

assumption made in conducting this kind of error analysis is that the results are consistent

with what the analytic values of the S-matrix elements would be provided they were

known for the case of the trapezoidal potential shown in Figure 13. The assumption,

however, is not unreasonable considering that previous results described in this thesis

indicated that for small Δx the curves behave like the analytic solutions. The results of

the next section will show that the amplitude of these oscillations weakens as the correct

Møller states are approached.

6.2   Results

The time for which the states were propagated was increased from $t = 4 \times 10^4$ to

8×10^5 atomic units in increments of 8.0×10^4. The potential used to perform these

---

[2] Ringing is also observed when the correlation function is not allowed to go back to zero and at energy

values not defined within the energy spread associated with the initial wave packets.

simulations is depicted in Figure 13 as the dashed trapezoidal well. As discussed earlier the amplitude of the ringing should diminish the longer the product and reactant wave packets are propagated away from the interaction region. In order try and incorporate any shift in phase or frequency an average of the amplitude of five oscillations present in each case was measured. An example of the oscillations used is shown in Figure 17. The general trend is that the amplitudes of the oscillations are smaller at higher energies. Therefore, if one can show that the average of these oscillations goes to zero as the time of propagation is increased a logical assertion would be that the oscillations
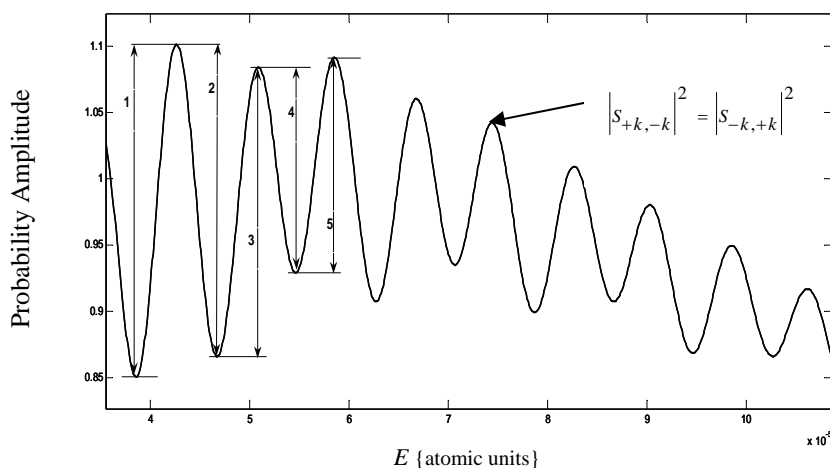
Figure 17. $S_{+k,-k}$ and $S_{-k,+k}$ curves showing the oscillations used to perform the error analysis.

which were not measured decrease as well. The results are shown in Figure 18. The average amplitude of the five oscillations was measured and plotted as a function of the time for which the products and reactants were propagated during the formation of the approximate Møller states.

45

The results shown in Figure 18 underscore the assertion that the oscillations decrease the further in time the product and reactant states are propagated away from the interaction region. A linear fit to the data gives a crude indicator of the time needed to diminish the ringing to some reasonable tolerance. Assuming that the simulated results match the analytic solution for the trapezoidal potential well used to perform these calculations, these results indicate that the algorithm converges to the correct S-matrix values as the true Møller states are approached.

It would then be reasonable to assume that if the trapezoidal potential well solution was known the computed S-matrix elements would be close to the analytic values. However, as with any hypothesis definitive proof is necessary to validate the assumptions. As such, it was necessary to determine the analytic transmission and reflection coefficients for a trapezoidal well.
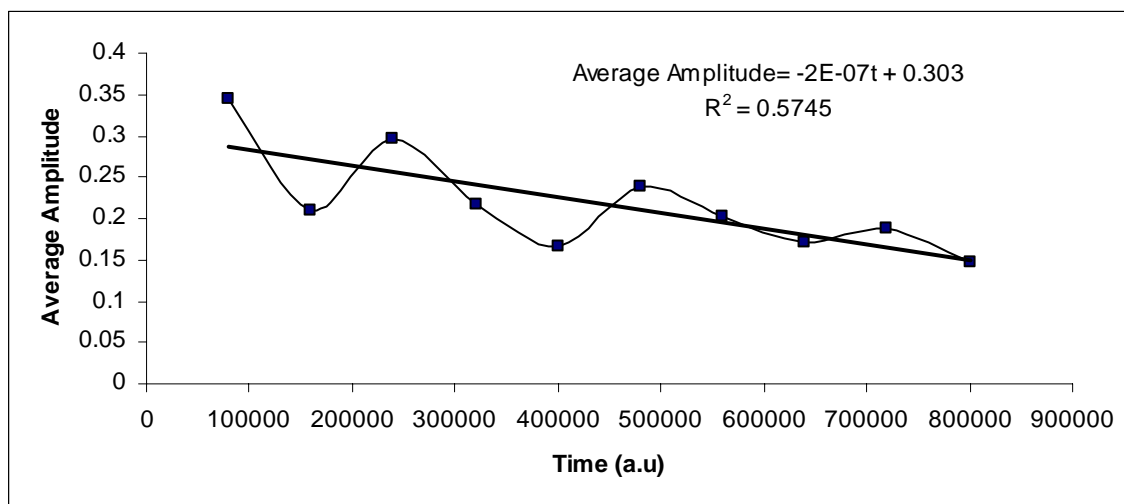
Figure 18. Average amplitude of the five oscillations shown in Figure 17 vs. the time for which the product and reactants were propagated away from the interaction region.

VII   Low-Energy Scattering (Trapezoidal Well)

7.1   Solving Schrödinger's Equation

Schrödinger's equation for a trapezoidal potential well contains the potential,

$$V(x, \Delta x) = \begin{cases} 0 & x \leq -a \\ -\dfrac{V_o}{\Delta x}(x+a) & -a < x < -a + \Delta x \\ -V_o & -a + \Delta x \leq x \leq a - \Delta x \\ \dfrac{V_o}{\Delta x}(x-a) & a - \Delta x < x < a \\ 0 & x \geq a \end{cases} \tag{57}$$

and is shown below.
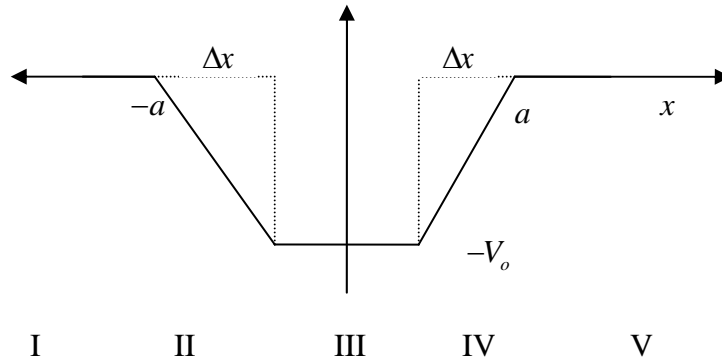
Figure 19. Trapezoidal potential showing effect of having a large Δx. The five regions are labeled under their respective parts.

The standard approach is to match boundary conditions across the five regions. The

solutions in regions (I, III, and V) are plane waves while regions (II and IV) contain Airy

functions. Mathematica was used to symbolically solve for T and R in terms of

$\Delta x, a,$ and E (Appendix B). The transmission coefficient was checked by comparing a

large Δx and very small Δx to a square well potential of length $2a = 4$. If the trapezoidal expression is correct it should approach a square well solution as Δx gets small. It was also verified that $T + R = 1$. The results of these tests are shown in Figures 20 and 21. Comparing Figures 20 and 21 it is apparent that the trapezoidal solution approaches the square well as Δx gets small. Figure 22 also reveals that the sum of the transmission and reflection coefficients is equal to one. These observations underscore the predicted expectations of the correct solution, and therefore the solution was taken to be acceptable.

(a)   (b)

(c)
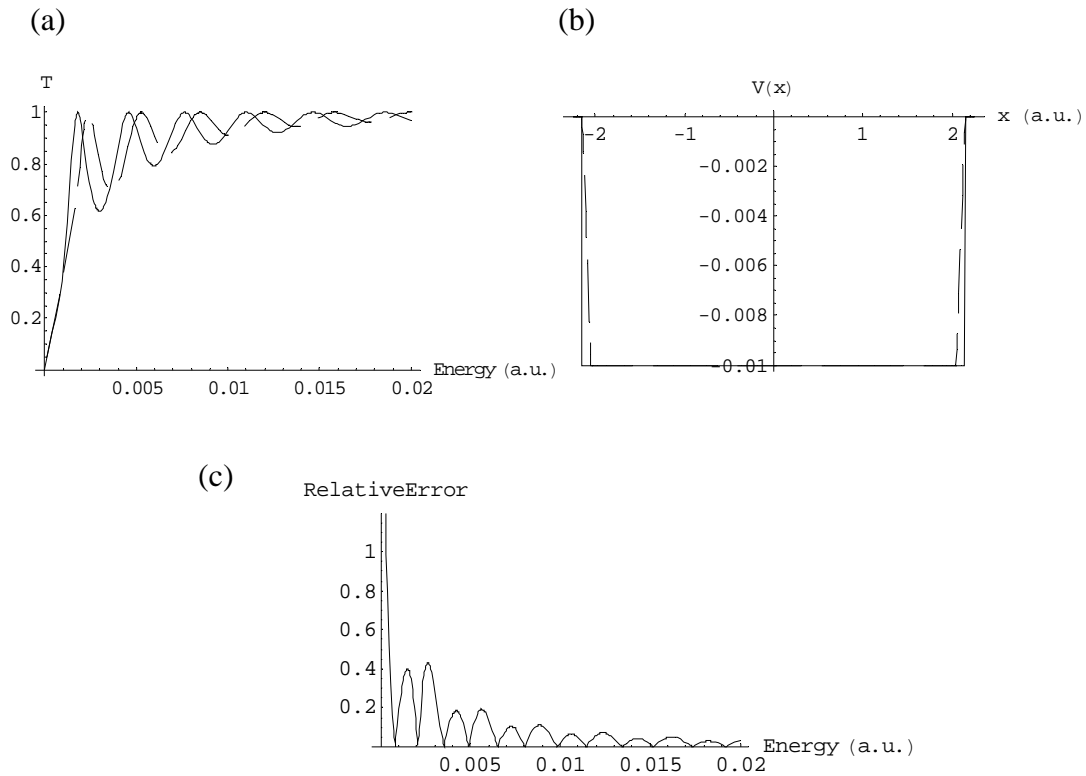
Figure 20. (a)Plot of the Transmission coefficient vs. energy (a.u.) for a square well (solid line) and trapezoidal well (dashed) with $\Delta x = 0.1$ (a.u.) (b) Plot showing the comparison of the trapezoidal potential and a square potential. (c) Relative error of the trapezoidal transmission coefficient and square well vs. energy (a.u.)

(a)

(b)

(c)
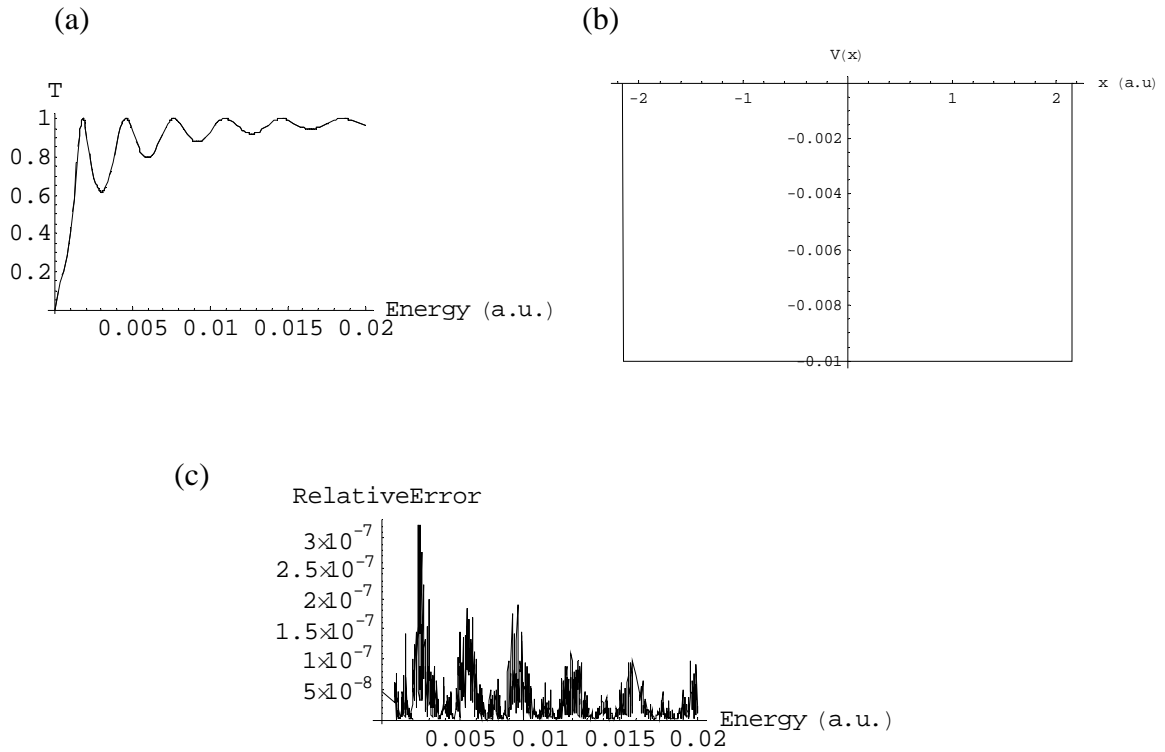
Figure 21. (a)Plot of the Transmission coefficient vs. energy (a.u.) for a square well (solid line) and trapezoidal well (dashed) with $\Delta x = \varepsilon$ (Machine Epsilon). (b) Plot showing the comparison of the trapezoidal potential and a square potential. (c) Relative error of the trapezoidal transmission coefficient and square well vs. energy (a.u.)
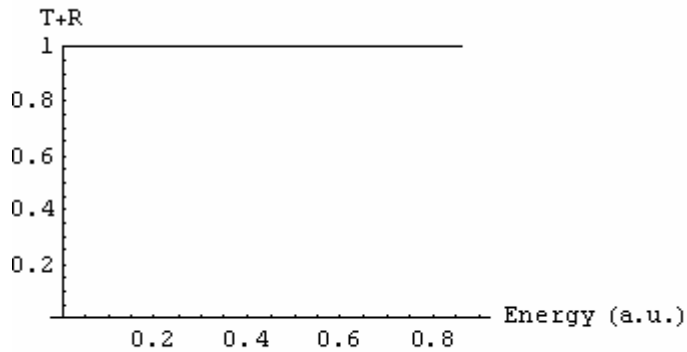
Figure 22. Plot of the T+R vs. Energy (a.u.) showing that it indeed equals one for all energies

49

VIII   Trapezoidal Well Error Analysis

Having the known analytic solution for a trapezoidal well allows a large grid as well as a large Δx value. The only requirement is that the linear regions of the trapezoidal representation are sampled well. The wave packets were set up as described in Figures 7 and 8 except with the trapezoidal potential shown below
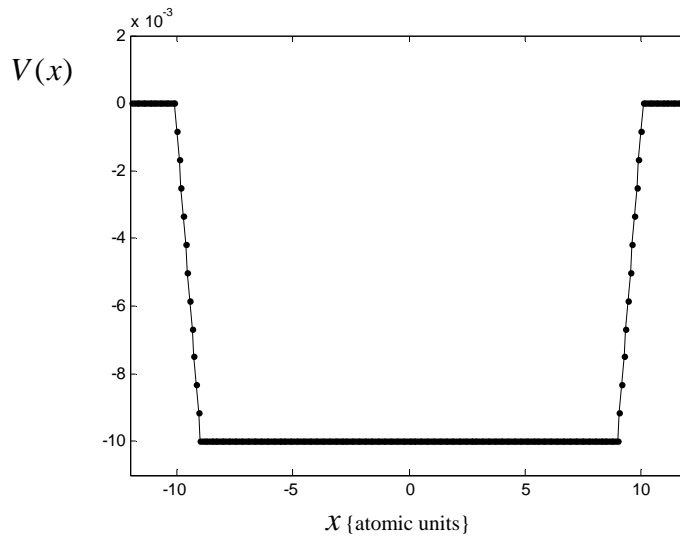
Figure 23. Trapezoidal potential well showing discrete
points along curve. The well is 0.01 atomic units deep.

Four tests were run at increasing times to determine if the algorithm's results converged to the analytic solution as the wave packets were propagated away from the interaction region. A sample calculation showing the transmission and reflection curves is shown in Figure 24. Notice that the same oscillatory nature seen earlier is present. However, these results are different than those of Figure 14 in that the simulated results are nearly an exact match outside the "ringing" portions; convergence to the analytic solution would be more accurate if one samples more points along the linear portions.
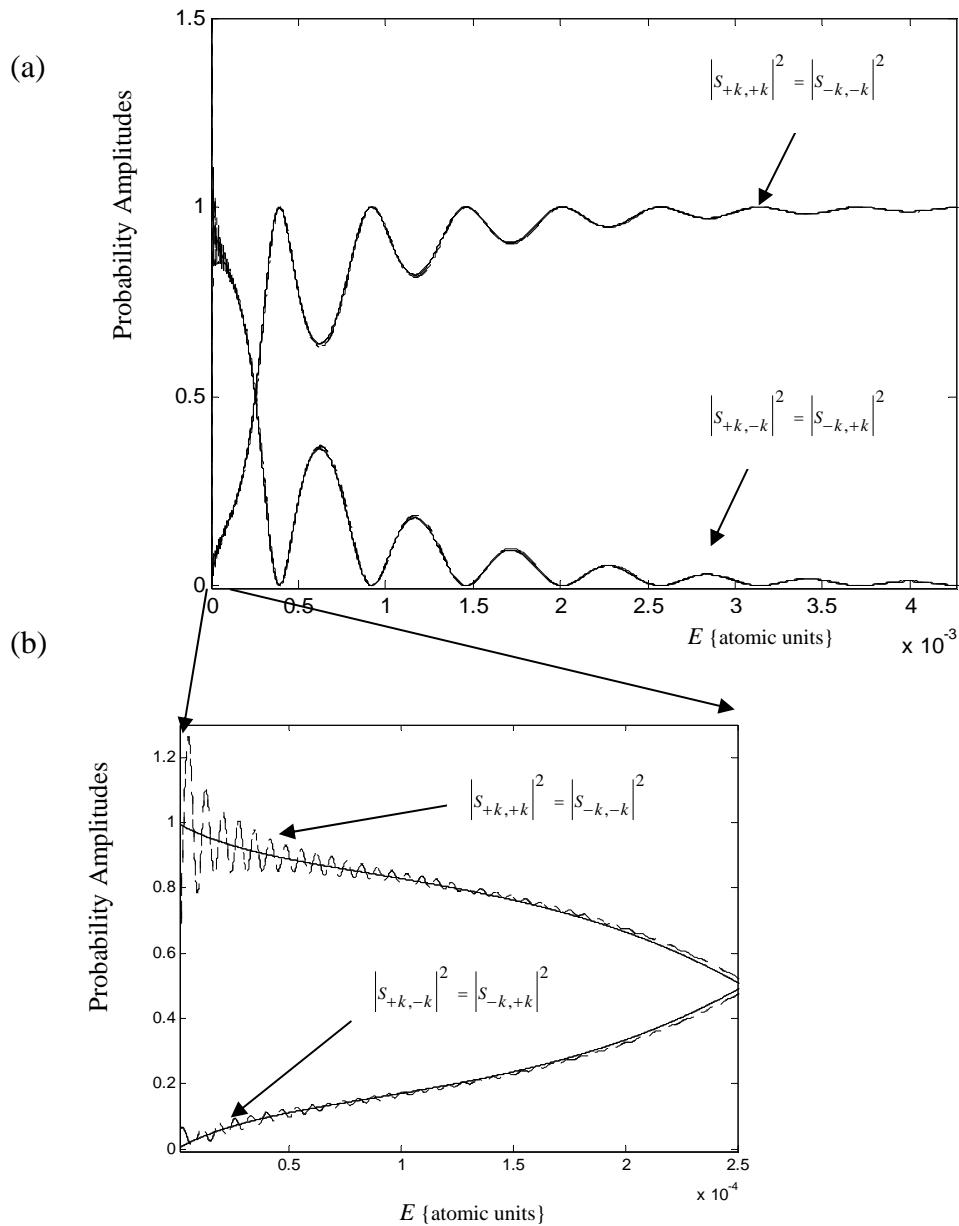
Figure 24. (a) Transmission [$S_{+k,+k}$, $S_{-k,-k}$] and reflection [$S_{+k,+k}$, $S_{-k,-k}$] curves for the trapezoidal well. The analytic solutions are (solid) while the simulated results are (dashed). (b) Zoomed in portion of low energy region showing oscillatory behavior.

An error analysis was done by summing the difference between the simulated results

and the analytic solution over the region for which ringing was observed:

51

$$\delta_R = \sum_{j=\alpha}^{\beta} \left(\left| S_{+k-k}(E_j) \right|^2 - R(E_j) \right)^2,$$ (58)

and
$$\delta_T = \sum_{j=\alpha}^{\beta} \left(\left| S_{+k+k}(E_j) \right|^2 - T(E_j) \right)^2,$$ (59)

where $E_\alpha = 1.15 \times 10^{-7}$ and $E_\beta = 2.5 \times 10^{-4}$ describe the first and last elements in the energy

array for which oscillations were measured, R and T denote the analytic reflection and

transmission coefficients for a trapezoidal well, and δ_R and δ_T denote the summation of

the error associated with reflection and transmission. The portion of the curves outside

the region for which ringing was seen was not included in the summation since the error

was negligible there.

8.1 Results

Measurements were taken using the results of four simulations for which the

products and reactants were propagated away from the interaction region. A table of the

times used is shown in table 2. A plot of δ_R and δ_T vs. the times listed in table 2 is shown

in Figure 25 along with a trend line showing that the summation errors go as

$$\delta_{R,T} = At^\gamma.$$ (60)

Notice that for both reflection and transmission the error converges as the time is

increased. The error associated with transmission is lower than the reflection error for all

times; in agreement with the previous error analysis. While it is not exactly clear how the

error made in the Møller states characterizes the error made in the transmission and

reflection curves, it is apparent that the closer one gets to making the correct Møller states

the closer both curves become to the analytic solutions.

52

Test 1	$t = 250000\ a.u$
Test 2	$t = 500000\ a.u$
Test3	$t = 750000\ a.u$
Test4	$t = 1000000\ a.u$

Table 2. Times of propagation for Error

Analysis Two

$$\delta_R = 6 \times 10^6 \, t^{-0.81}$$

$$R^2 = 0.999$$

$$\delta_T = 3 \times 10^{13} \, t^{-2.16}$$

$$R^2 = 0.997$$

t {atomic units}
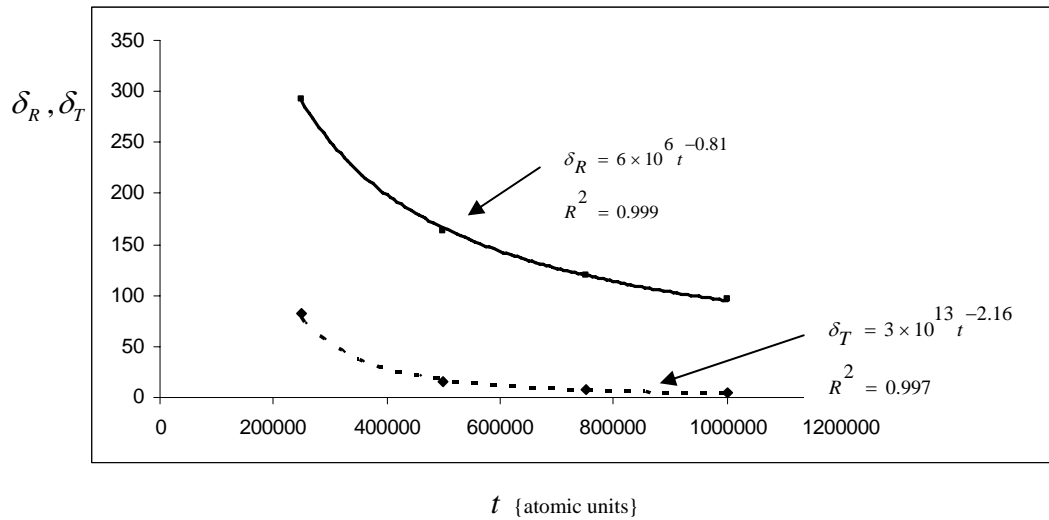
Figure 25. δ_R (solid) and δ_T (dashed) vs. time along with power fits showing convergence.

To test the assertion that the ringing seen in the low energy portion of the transmission and reflection curves is caused by using incorrect Møller states we measured the area of the residual wave packet left inside the interaction region at the time the approximate intermediate Møller states were formed. At each time listed in table 2 the area under the curve described by the free particle, time- evolving Gaussian wave packet

53

described by equation (26)was measured (Figure 26). Since the analytic form was known the propagations as well as the integrals were performed analytically.
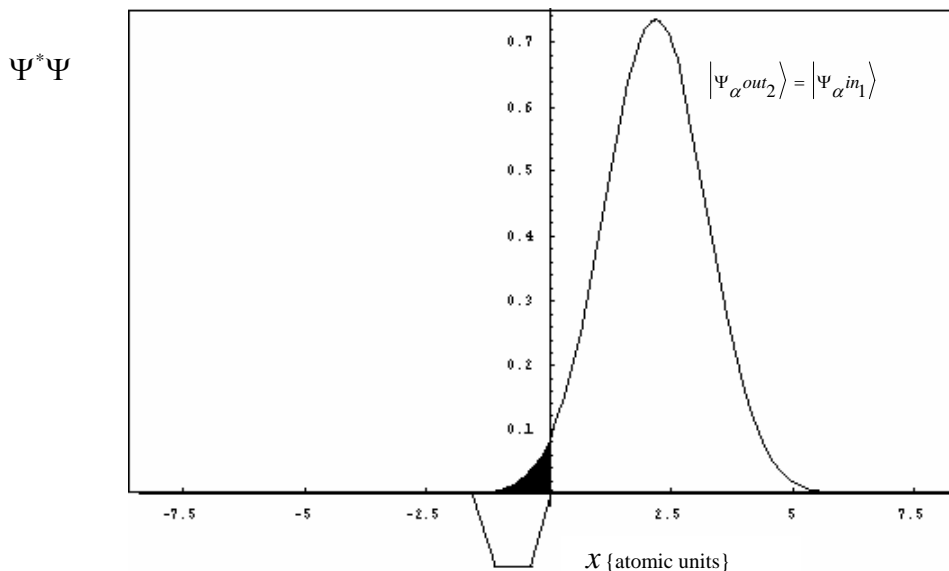
Figure 26. Schematic showing integrated residue (shaded) inside interaction potential (Trapezoidal Well).

The results are plotted in Figure 27 along with the previous plots δ_R and δ_T. The integrated data was scaled such that the point at $t = 1 \times 10^6$ matched $\delta_R(t = 1 \times 10^6)$ and $\delta_T(t = 1 \times 10^6)$; the same scaling factor was then applied to the other three data points. Since the data was scaled to have the points at $t = 1 \times 10^6$ match, the integrated data is more closely related to the relative error curves at longer times. If the points at $t = 2.5 \times 10^5$ were scaled to match the plots would indicate a stronger correlation at shorter times. Although the scaling is arbitrary the empirical results shown in Figure 27 underscore the assertion that the error seen in the ringing is related to the residual tail left inside the interaction region during the construction of the Møller states.

54
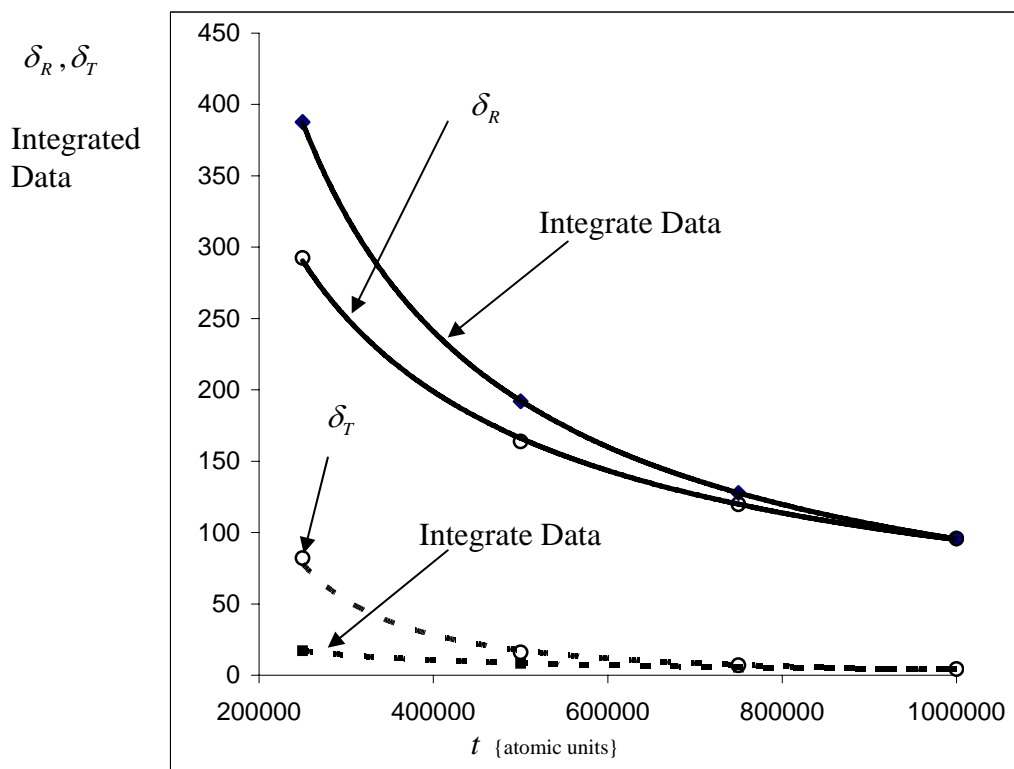
Figure 27. δ_R & δ_T along with the integrated data showing the correlation between residue left inside interaction region and error associated with ringing.

The most probable explanation for the offsets is that the error associated with the

incorrect Møller states is propagated through the rest of the CPM method (ie. correlation

function, Fourier transforms, and the S-matrix elements). Both curves show the

drawback of this approach in that it requires long propagation times to achieve little error

in the low energy regions.

IX   Conclusion

This thesis contributes to the understanding of the Channel Packet method and low-energy, time dependent scattering theory. Two properties of this thesis make it ideal for understanding the complications associated with the low energy problem. The first is that it demonstrates the need for a four-by-four matrix of expansion coefficients to handle wave packets which contain positive and negative momentum. In doing so however, one must accept the increased complexity of solving all four S-matrix elements at once. The second property is that this thesis explains the difficulty in constructing the Møller states from reactant and product wave packets which contain both positive and negative momentum.

The thesis extended the application of the CPM to tackle the specific problem of low energy scattering. A new algorithm was presented which relaxes the requirement that the product and reactant wave packets only contain positive or negative momentum. In doing so, the algorithm allows wave packets to be fully represented across the entire energy range. The requirements to solve the low energy problem are now completely understood. The first requirement is that the product and reactant wave packets contain both positive and negative momentum. The second requirement is that the correct Møller states must be used. While the technique presented in this paper meets the first requirement, the latter was never obtained. However, this thesis demonstrated that as the proper Møller states are approached the oscillations diminish and the correct S-matrix elements are approached. It was shown that to accurately construct the Møller states will require a very large grid, and that the main downside to the approach taken in this thesis

is that one must accept very long simulation times. However, as technology increases and processors become faster this algorithm may become the algorithm of choice for time dependent scattering theory. This thesis explained the difficulties associated with low energy, time dependent scattering theory as well as a new approach which significantly improves the calculation of the low-energy S-matrix elements. The thesis demonstrated that the new approach will work but at a high computational price. Finally, if one is only interested in high energy scattering using the previous approaches described in [1-3] is simpler. However, if one needs to characterize low energy scattering the algorithm described in this thesis is a valid approach.

Ideas for further research include investigating how one could avoid using very large grids when the products and reactants contain positive and negative momentum. One possible solution may be that during the second half of the Møller operator, the propagations under the full Hamiltonian, the Gaussian wave packets could be "created" at the boundaries of a smaller grid at each time step as they moved back into the interaction region. The split operator would need to be modified to accept certain boundary conditions at the ends of the grid. If one could construct the algorithm using small grids the computation time needed to perform the simulations would be greatly reduced.

Appendix A. The Trotter Theorem (Split-Operator Approximation)

The time evolution operator

$$\hat{U} = \exp\left[-i\frac{\Delta t}{\hbar}(\hat{T}+\hat{V})\right] \tag{A.1}$$

cannot be split according to

$$\exp\left[-i\frac{\Delta t}{\hbar}(\hat{T}+\hat{V})\right] \neq \exp\left(-i\frac{\Delta t}{\hbar}\hat{T}\right)\exp\left(-i\frac{\Delta t}{\hbar}\hat{V}\right), \tag{A.2}$$

since $\left[\hat{T},\hat{V}\right] \neq 0$. In order to split the operator one must approximate a new operator

using the Trotter theorem, which states that [13]

$$\exp[i(L_1+L_2)t] = \lim_{M\to\infty}\left[\exp\left(\frac{iL_2t}{2M}\right)\exp\left(\frac{iL_1t}{M}\right)\exp\left(\frac{iL_2t}{2M}\right)\right]^M, \tag{A.3}$$

where L_1 and L_2 are general Liouville operators. If one allows M to be large, but finite :

$$\exp[i(L_1+L_2)t] \approx \left[\exp\left(\frac{iL_2t}{2M}\right)\exp\left(\frac{iL_1t}{M}\right)\exp\left(\frac{iL_2t}{2M}\right)\right]^M, \tag{A.4}$$

which can be rearranged by taking the M_{th} root to give

$$\exp\left[i(L_1+L_2)\frac{t}{M}\right] \approx \left[\exp\left(\frac{iL_2t}{2M}\right)\exp\left(\frac{iL_1t}{M}\right)\exp\left(\frac{iL_2t}{2M}\right)\right]. \tag{A.5}$$

Interpreting t/M as a single time step, Δt, and replacing L_1 and L_2 with $-\dfrac{\hat{V}}{\hbar}$ and $-\dfrac{\hat{T}}{\hbar}$ a

single-time-step, approximate propagator may be written as

$$\hat{P}(\Delta t) = \left[\exp\left(\frac{-i\hat{T}}{2\hbar} \Delta t \right) \exp\left(-\frac{i\hat{V}}{\hbar} \Delta t \right) \exp\left(\frac{-i\hat{T}}{2\hbar} \Delta t \right) \right]. \tag{A.6}$$

This operator is unitary and thus preserves time reversibility:

$$\hat{P}^\dagger(\Delta t) = \hat{P}(-\Delta t) = \hat{P}^{-1}(\Delta t) \ , \tag{A.7}$$

$$\hat{P}(-\Delta t)\hat{P}(\Delta t) = I. \tag{A.8}$$

Using a Taylor expansion $\hat{P}(\Delta t)$ is accurate to order Δt^2 :

$$\exp\left(\frac{-i\hat{T}}{2\hbar} \Delta t \right) \exp\left(-\frac{i\hat{V}}{\hbar} \Delta t \right) \exp\left(\frac{-i\hat{T}}{2\hbar} \Delta t \right) = 1 - \frac{i(\hat{T}+\hat{V})}{\hbar} \Delta t - \frac{(\hat{T}+\hat{V})^2}{2\hbar^2} \Delta t^2 + O[\Delta t]^3$$

$$\approx \exp\left(-\frac{i\hat{H}}{\hbar} \Delta t \right). \tag{A.9}$$

Hence, $\hat{P}(\Delta t) = \hat{U}(\Delta t)$ up to second order in Δt . One can then interpret that the

propagator is stable under the requirement

$$E_{max} \Delta t \ll 1 \ , \tag{A.10}$$

where $E_{max} = T_{max} + V_{max}$.

Appendix B. Trapezoidal Well Transmission and Reflection Coefficients

```
In[1]:= ClearAll[a, Vo , Δx , m , hbar]

        V1 = 0;
        V2 = - Vo/Δx * (x + a);
        V3 = -Vo;
        V4 = Vo/Δx * (x - a);
        V5 = 0;
        k = √(2 * m * T) / hbar ;
        l = √(2 * m * (T + Vo)) / hbar ;
```

```
In[9]:= region1[x_] = A * Exp[i * k * x] + B * Exp[-i * k * x]
```

$$\text{Out[9]= } B\, e^{-\frac{i\sqrt{2}\sqrt{m T}\, x}{hbar}} + A\, e^{\frac{i\sqrt{2}\sqrt{m T}\, x}{hbar}}$$

```
In[10]:=
        ans2 = Assuming[T > 0, DSolve[Φ''[x] == - (2 * m * (T - V2))/hbar² * Φ[x], Φ[x], x, GeneratedParameters → B]]
        region2[x_] = ans2[[1, 1, 2]]
```

$$\text{Out[10]= } \left\{\left\{\Phi[x] \to AiryAi\left[\frac{-\frac{2 m Vo\, x}{hbar^2 \Delta x} - \frac{2 (a m Vo + m T \Delta x)}{hbar^2 \Delta x}}{2^{2/3}\left(-\frac{m Vo}{hbar^2 \Delta x}\right)^{2/3}}\right] B[1] + AiryBi\left[\frac{-\frac{2 m Vo\, x}{hbar^2 \Delta x} - \frac{2(a m Vo + m T \Delta x)}{hbar^2 \Delta x}}{2^{2/3}\left(-\frac{m Vo}{hbar^2 \Delta x}\right)^{2/3}}\right] B[2]\right\}\right\}$$

$$\text{Out[11]= } AiryAi\left[\frac{-\frac{2 m Vo\, x}{hbar^2 \Delta x} - \frac{2(a m Vo + m T \Delta x)}{hbar^2 \Delta x}}{2^{2/3}\left(-\frac{m Vo}{hbar^2 \Delta x}\right)^{2/3}}\right] B[1] + AiryBi\left[\frac{-\frac{2 m Vo\, x}{hbar^2 \Delta x} - \frac{2(a m Vo + m T \Delta x)}{hbar^2 \Delta x}}{2^{2/3}\left(-\frac{m Vo}{hbar^2 \Delta x}\right)^{2/3}}\right] B[2]$$

```
In[12]:=
        region3[x_] = D1 * Sin[l * x] + D2 * Cos[l * x]
```

$$\text{Out[12]= } D2\, Cos\left[\frac{\sqrt{2}\sqrt{m(T+Vo)}\, x}{hbar}\right] + D1\, Sin\left[\frac{\sqrt{2}\sqrt{m(T+Vo)}\, x}{hbar}\right]$$

```
In[13]:=
        ans4 = Assuming[T > 0, DSolve[Φ''[x] == (-2 * m * (T - V4))/hbar² * Φ[x], Φ[x], x, GeneratedParameters → M]]
        region4[x_] = ans4[[1, 1, 2]];
```

$$\text{Out[13]= } \left\{\left\{\Phi[x] \to AiryAi\left[\frac{\frac{2 m Vo\, x}{hbar^2 \Delta x} - \frac{2(a m Vo + m T \Delta x)}{hbar^2 \Delta x}}{2^{2/3}\left(\frac{m Vo}{hbar^2 \Delta x}\right)^{2/3}}\right] M[1] + AiryBi\left[\frac{\frac{2 m Vo\, x}{hbar^2 \Delta x} - \frac{2(a m Vo + m T \Delta x)}{hbar^2 \Delta x}}{2^{2/3}\left(\frac{m Vo}{hbar^2 \Delta x}\right)^{2/3}}\right] M[2]\right\}\right\}$$

```
In[15]:=
        region5[x_] = F * Exp[i * k * x]
```

$$\text{Out[15]= } e^{\frac{i\sqrt{2}\sqrt{m T}\, x}{hbar}}\, F$$

```
In[16]:=
        ans1 = Solve[{region4'[a] == region5'[a], region4[a] == region5[a]}, {M[1], M[2]}];
        "This Solves for M1 and M2 in terms of F"

        M1 = ans1[[1, 1, 2]];
        M2 = ans1[[1, 2, 2]];
```

```
Out[17]= This Solves for M1 and M2 in terms of F
```

```
In[20]:= ans2 = Solve[{region3'[a - Δx] == region4'[a - Δx], region3[a - Δx] == region4[a - Δx]}, {D1, D2}] /.
            {M[1] -> M1, M[2] → M2};
        S1 = ans2[[1, 1, 2]];
        S2 = ans2[[1, 2, 2]];
        "This solves for D1 and D2 in terms of F"
```

```
Out[23]= This solves for D1 and D2 in terms of F
```

```
In[24]:= ans3 = Solve[{region2'[-a + Δx] == region3'[-a + Δx], region2[-a + Δx] == region3[-a + Δx]}, {B[1], B[2]}] /.
            {D1 → S1, D2 → S2};
        B1 = ans3[[1, 1, 2]];
        B2 = ans3[[1, 2, 2]];
        "this solves for B1 and B2 in terms of F"
```

```
Out[27]= this solves for B1 and B2 in terms of F
```

```
In[28]:=
        ans4 = Solve[{region1'[-a] == region2'[-a], region1[-a] == region2[-a]}, {B, A}] /. {B[1] → B1, B[2] → B2};
        Bnew = ans4[[1, 1, 2]];
        Anew = ans4[[1, 2, 2]];
        "Finally this solves for B and A in terms of F"
```

```
Out[31]= Finally this solves for B and A in terms of F
```

```
In[36]:=
        Transmission[T_, Δx_] = Abs[F / Factor[Anew]] ^ 2;
        Reflection[T_, Δx_] = Abs[Factor[Bnew / Anew]] ^ 2;
```

60

Appendix C (Simulation Parameters)

$x_{\substack{\text{min} \\ \text{max}}} = \mp 1200$	$m = 1833.35$
$\Delta t = 1$	$\Delta x \approx 0.092$
$\sigma_{x_o} = 0.5$	$\Delta k \approx 0.00026$
$N = 2^{18}$	$V_o = -0.01$
$k_{\text{max}} \approx 34.1$	$E_{\text{max}} \approx 0.03$ $E_{\text{min}} \approx 1.12 \times 10^{-7}$

Table. 3 Sample parameters of simulation for $k_o = \pm 4$

Bibliography

1. D.J. Tannor and D.E. Weeks, J. Chem. Phys. 98 (1993).

2. D.E. Weeks and D.J. Tannor, Chem. Phys. Letters 207 (1993).

3. D.E. Weeks and D.J. Tannor, Chem. Phys. Letters 224 1994.

4. Griffiths, David J. *An Introduction to Quantum Mechanics.* Prentice Hall, 2nd edition, (1995).

5. Asmar, Nakhle H. *Partial Differential Equations.* Pearson Prentice Hall, 2nd edition, (2000).

6. D.E. Weeks, Lecture Notes. *S-Matrix Lecture #2.* [4]

7. J. Taylor, *Scattering Theory: The Quantum Theory of Nonrelativistic Collisions* (Wiley, New York, 1972).

8. Liboff, Richard L. *Introductory Quantum Mechanics.* Addison Wesley, 4th edition, (2003).

9. V. Engel and H. Metiu, J. Chem. Phys. (89) (1988) 1986.

10. Burden, Richard L. and J. Dougless Fares. *Numerical Analysis.* Thompson Brooks Cole, (2005).

11. Pratap, Rudra. *Getting Started With Matlab.* Oxford University Press, (2006)

12. Wolfson, Richard, and Jay M. Pasachoff. *Physics for Scientists and Engineers.* Addison-Wesley 3rd edition, (1999).

13. L. S. Schulman, Techniques and Applications of Path Integration (Wiley, New York, 1996), Append. to Ch. 1.

Vita

Second Lieutenant Clint Zeringue graduated from Germantown High School in Germantown, Tennessee. He was earned an appointment to the United States Air Force Academy where he was commissioned and received a Bachelor of Science degree in Physics in June 2005. That same year he entered the Graduate School of Engineering and Management; Department of Engineering Physics at the Air Force Institute of Technology, Wright Patterson AFB. After graduation he will be assigned to the Air Force Research Laboratory at Kirtland AFB, New Mexico.

REPORT DOCUMENTATION PAGE				*Form Approved* *OMB No. 074-0188*

The public reporting burden for this collection of information is estimated to average 1 hour per response, including the time for reviewing instructions, searching existing data sources, gathering and maintaining the data needed, and completing and reviewing the collection of information. Send comments regarding this burden estimate or any other aspect of the collection of information, including suggestions for reducing this burden to Department of Defense, Washington Headquarters Services, Directorate for Information Operations and Reports (0704-0188), 1215 Jefferson Davis Highway, Suite 1204, Arlington, VA 22202-4302. Respondents should be aware that notwithstanding any other provision of law, no person shall be subject to an penalty for failing to comply with a collection of information if it does not display a currently valid OMB control number.
PLEASE DO NOT RETURN YOUR FORM TO THE ABOVE ADDRESS.

1. REPORT DATE *(DD-MM-YYYY)* 07-Sept-2006	2. REPORT TYPE Master's Thesis	3. DATES COVERED *(From – To)* Nov. 2005 – Sept 2006

4. TITLE AND SUBTITLE A New Application of the Channel Packet Method for Low Energy 1-D Elastic Scattering	5a. CONTRACT NUMBER
	5b. GRANT NUMBER
	5c. PROGRAM ELEMENT NUMBER
6. AUTHOR(S) Zeringue, Clint M., Second Lieutenant, USAF	5d. PROJECT NUMBER
	5e. TASK NUMBER
	5f. WORK UNIT NUMBER

7. PERFORMING ORGANIZATION NAMES(S) AND ADDRESS(S) Air Force Institute of Technology Graduate School of Engineering and Management (AFIT/EN) 2950 Hobson Way, Building 640 WPAFB OH 45433-8865	8. PERFORMING ORGANIZATION REPORT NUMBER AFIT/GAP/ENP/06-22

9. SPONSORING/MONITORING AGENCY NAME(S) AND ADDRESS(ES) N/A	10. SPONSOR/MONITOR'S ACRONYM(S)
	11. SPONSOR/MONITOR'S REPORT NUMBER(S)

12. DISTRIBUTION/AVAILABILITY STATEMENT

APPROVED FOR PUBLIC RELEASE; DISTRIBUTION UNLIMITED.

13. SUPPLEMENTARY NOTES

14. ABSTRACT

An algorithm is presented which uses the channel packet method (CPM) to simulate low-energy, wave-packet propagation and compute S-matrix elements. A four-by-four matrix containing the momentum, expansion coefficients of the reactants and products is introduced to account for initial and final states having both positive and negative momentum. The approach does not consider scattering from one side or the other, rather it considers both incoming and outgoing wave packets from the left and right simultaneously. Therefore, during one simulation all four S-matrix elements, $S_{++}, S_{+-}, S_{-+},$ and S_{--} are computed.

Numerical simulations of the algorithm are carried out on a conventional desktop computer and compared to the analytic solution of the transmission and reflection functions for a square well. The simulated results agree very well with the known solution up until very low energies, after which the results begin to oscillate about the theoretical values. The results indicate that if the correct Møller states are used the algorithm will produce the correct S-matrix elements across the entire energy range.

15. SUBJECT TERMS

Time-Dependent Scattering Theory, Channel Packet Method, Square Well, Trapezoidal Well, Low-Energy Scattering, S-Matrix, Algorithms

16. SECURITY CLASSIFICATION OF:			17. LIMITATION OF ABSTRACT	18. NUMBER OF PAGES	19a. NAME OF RESPONSIBLE PERSON David E. Weeks
a. REPORT	b. ABSTRACT	c. THIS PAGE	UU	75	19b. TELEPHONE NUMBER *(Include area code)* (937) 255-6565 ext 4561 (david.weeks@afit.edu)
U	U	U			